Extended chronologies of aqueous alteration in the CM2 carbonaceous chondrites: Evidence from carbonates in Queen Alexandra Range 93005

M. R. Lee[a*], P. Lindgren[a], M. R. Sofe[a], C. M. O'D Alexander[b] and J. Wang[b]
[a]*School of Geographical and Earth Sciences, University of Glasgow, Gregory Building, Lilybank Gardens, Glasgow G12 8QQ, U.K.* [b]*Department of Terrestrial Magnetism, Carnegie Institution of Washington, 5241 Broad Branch Road, NW, Washington, DC 20015, USA.*
*Corresponding author. E-mail address: Martin.Lee@Glasgow.ac.uk

Abstract

The Antarctic CM2 carbonaceous chondrite QUE 93005 contains four compositionally distinct carbonates, namely breunnerite, calcite, dolomite and a Ca-poor dolomite. These carbonates can form monomineralic grains, or may be intergrown as bimineralic grains consisting of dolomite plus breunnerite and dolomite plus calcite, or polymineralic grains containing an intergrowth of breunnerite, Ca-poor dolomite and calcite. Carbonates in all grain types have inclusions of Fe,Ni sulphides and/or Mg-Fe phyllosilicates. In the bimineralic grains dolomite crystallised first to be overgrown by breunnerite or partially replaced by calcite. Polymineralic grains are concentrically layered, with breunnerite crystallising first on pore margins to be later etched, then overgrown and partially replaced by Ca-poor dolomite that was itself partly dissolved prior to being overgrown by calcite. Calcite and dolomite have also cemented fractures that cross-cut the fine-grained rims to aqueously altered chondrules and were formed by expansion of the chondrules during their hydration. Overall, the sequence of mineralisation in QUE 93005 was: (1) dolomite, (2) breunnerite, (3) Ca-poor dolomite then (4) calcite. This secular change in carbonate composition and mineralogy reflects changing solution composition and probably also provenance. Mg-Fe phyllosilicates replaced dolomite, breunnerite and Ca-poor dolomite prior to calcite crystallisation and most or all of the sulphides formed after both the phyllosilicates and calcite. Following sulphide crystallisation the edges of carbonate grains were abraded, either by impact 'gardening' or as a consequence of fluidisation of the matrix during rapid loss of gas or vapour. Determination of the crystallisation age of dolomite via the Mn–Cr system indicates that aqueous alteration of QUE 93005 began on or before 3.93 ± 0.23 Ma after the formation of the solar system. Overall, the water/rock ratio and fO_2 during alteration of QUE 93005 was similar to that of the CM1s and CR1s, but the lower degree of alteration of QUE 93005 overall suggests that alteration timescales were shorter, possibly due to loss of intergranular liquid water during fluidisation.

1. INTRODUCTION

The CM carbonaceous chondrites contain evidence for extensive parent body aqueous alteration of their original silicates, oxides, metals, sulphides and amorphous constituents (e.g. Fuchs et al., 1973; Bunch and Chang, 1980; Tomeoka and Buseck, 1985; Brearley, 2006a). The products of this alteration are principally phyllosilicates, together with smaller quantities of sulphides, oxides and carbonates (McSween, 1979; Barber, 1981, 1985; Johnson and Prinz, 1993; Lee and Ellen, 2008; Howard et al., 2009, 2011). Despite their low volumetric abundances, the carbonates can potentially provide detailed information on mechanisms and histories of aqueous alteration. Their utility comes in part from their relatively coarse crystal size (tens to hundreds of micrometers), which makes them amenable to electron- and ion-beam imaging and analysis (e.g. Johnson and Prinz, 1993; Riciputi et al., 1994; Brearley 1998; Brearley et al., 1999, 2001; de Leuw et al., 2010). The solubility of these carbonates makes it easy to chemically separate them from their silicate-oxide-sulphide matrix by acid digestion for subsequent isotopic analysis (Grady et al., 1988; Benedix et al., 2003; Guo and Eiler, 2007). Furthermore, clear variations in the mineralogy and chemical and isotopic composition of carbonates within and between meteorites demonstrates that they have faithfully recorded the physico-chemical properties of aqueous solutions and so can reveal how they varied spatially and temporally (e.g. Johnson and Prinz, 1993; Riciputi et al., 1994; Benedix et al., 2003; de Leuw et al., 2010; Tyra et al., 2012).

Previous studies have found that most CM2 meteorites contain a single generation of carbonate that crystallised in a parent body environment and from low temperature (20-71°C) brines (Johnson and Prinz, 1993; Riciputi et al., 1994; Guo and Eiler, 2007). Although aqueous solutions are believed to have been essentially static (Bland et al., 2009), the trace element and isotopic zoning of individual grains shows that fluid compositions changed rapidly relative to crystallisation timescales (Brearley, 1998; Brearley et al., 1999, 2001, 2006; Lee and Ellen, 2008). Multiple chemically and isotopically distinct generations of calcite have however also been recorded from the CM2 meteorites LON 94101 (Lindgren et al., 2011) and EET 96006 (Tyra et al., 2012), thus demonstrating fluctuations in solution compositions over longer timescales.

Comparisons between the carbonate populations of different CM2 meteorites show that their mineralogy and chemical composition varies with the degree of alteration of their host rock. Ca carbonates are dominant in those meteorites that have been less heavily altered overall, with dolomite and other ‘complex’ Mg-Mn-Fe-Ni bearing carbonates comprising a greater proportion of the population in the highly altered CM2s (Riciputi et al., 1994; Zolensky et al., 1997; Rubin, et al., 2007; de Leuw et al., 2010). One interpretation of this correspondence between degree of aqueous alteration and carbonate chemistry and mineralogy is that calcite crystallised early, probably utilising Ca liberated from sources including chondrule mesostases (Brearley, 2006b) and the complex carbonates precipitated later and from pore fluids whose compositions had changed in response to dissolution of metals and ferromagnesian silicates (Riciputi et al., 1994). This model assumes that all of the CM2s studied had comparable initial compositions and were altered under similar physico-chemical conditions, although recent determinations of the modal mineralogy of a suite of CM2s has indicated that the group was initially more heterogeneous than previously assumed (Howard et al., 2009, 2011). Nonetheless, possible support for models invoking a genetic

link between carbonate mineralogy and degree of alteration comes from their crystallisation ages, as determined using the $^{53}Mn–^{53}Cr$ system, which show that calcite in the CM2s is older than breunnerite and dolomite in the more highly aqueously altered CI meteorites (e.g. Brearley and Hutcheon, 2000, 2002; de Leuw et al., 2009b). Overall, these observations suggest that with progressive aqueous alteration of a carbonaceous chondrite starting material the carbonate population evolves from being dominated by Ca-carbonates to containing a greater proportion of Mg- and Fe-rich carbonates. However, the processes by which the population of carbonate grains within a meteorite can change in its composition and mineralogy remains unknown.

Here we aim to test this model for the linked evolution of CM2 carbonates and their parent rocks by analysis of the highly aqueously altered CM2 Queen Alexandra Range (QUE) 93005. For these tests the petrographic context, mineralogy and chemical composition of carbonate minerals and associated alteration products has been characterised using a range of electron beam imaging and analysis techniques. The relative sequence of mineralisation obtained has also been anchored to quantitative chronologies by determining carbonate crystallisation ages using the $^{53}Mn–^{53}Cr$ system. QUE 93005 is especially useful for testing alteration models because it contains dolomite together with grains of Ca-carbonate rimmed by 'complex carbonates' (Rubin et al., 2007; de Leuw et al., 2010). In addition to potentially providing a quantitative mineralisation chronology from one parent body region, QUE 93005 can also be used to investigate how the mineralogy and composition of meteoritic carbonates may 'evolve' during aqueous alteration, and three processes can be hypothesised: (i) crystallisation of a sequence of pore-filling cements whose mineralogy and composition changes in step with solution chemistry, (ii) dissolution of one carbonate population followed by later precipitation of another, or (iii) replacement of an earlier carbonate generation by one that has crystallised from compositionally more evolved fluids. Our results reveal that QUE 93005 contains four generations of carbonates that provide a detailed record of changes in solution compositions during aqueous alteration and provide new insights into the scale and connectivity of the aqueous system. As the QUE93005 carbonates include breunnerite, they may also help to elucidate any evolutionary links between CM2s and other carbonaceous chondrites that contain Mg-Fe carbonates.

2. MATERIALS AND METHODS

2.1. QUE 93005

This meteorite is a 13.4g Antarctic find with a weathering grade of A/Be (Grossman and Score, 1996) and <2 (Rubin et al., 2007) . It was classified as a CM 2.1 by Rubin et al. (2007), and Velbel et al. (2005) noted that it has an approximate mineralogical alteration index of 0.7. Howard et al. (2011a) found that QUE 93005 contains 82% of hydrous phyllosilicates, which is greater than most other CM2s analysed by them, but less than CM2.0/CM1 meteorites (e.g. SCO 06043 contains 88% phyllosilicates). QUE 93005 carbonates have been previously described by de Leuw et al. (2006a, b, 2007, 2009a, b, 2010) and Rubin et al. (2007). They recorded 2-3 volume % that is distributed randomly throughout the meteorite matrix and comprises grains of Ca-carbonate (50-100 μm) and calcian dolomite (10-30 μm), the latter frequently rimmed by pentlandite.

2.2. Sample characterisation

This study used one 126 μm^2 petrographic thin section (QUE 93005,10) of QUE 93005 that is approximately semicircular in shape with a fusion crust along the curving edge. Backscattered electron (BSE) and cathodoluminescence (CL) images together with electron backscatter diffraction (EBSD) maps were acquired using a FEI Quanta 200F SEM operated at 20 kV and with a high beam current (beam currents are not quantified by this instrument). The SEM is equipped with a KE developments panchromatic CL detector and an EDAX-TSL EBSD system. Prior to EBSD work, the thin section was briefly repolished in colloidal silica in order to enhance Kikuchi pattern quality and all EBSD maps were acquired from the uncoated thin section with the SEM operated at low vacuum (~60 Pa). The Kikuchi patterns were indexed using structure files for calcite ($R\bar{3}c$: a= 0.4991 nm, b = 0.4991 nm, c = 1.7062 nm, $\beta = 120^o$) and dolomite ($R\bar{3}$: a= 0.4807 nm, b = 0.4807 nm, c = 1.6010 nm, $\beta = 120^o$). The orientation of the calcite or dolomite *c* axis (i.e. the pole to (0001) planes) and the *a* axes (i.e. the poles to $\{2\bar{1}\bar{1}0\}$ planes) are plotted as stereographic upper hemisphere pole figures.

2.3. X-ray microanalysis

For quantitative chemical analyses two instruments were used. One dataset was obtained with a Zeiss Sigma field-emission scanning electron microscope (FEG-SEM) equipped with an Oxford Instruments X-Max 80 mm^2 silicon-drift energy-dispersive X-ray (EDX) detector. Spectra were acquired at 15 kV/2 nA with the electron beam rastered over an area of ~ 5 μm^2, and the counting time was 60 secs. Spectra were quantified with an Oxford Instruments INCA microanalysis system and calibration used the following mineral standards: calcite (Ca), periclase (Mg), pyrite (S and Fe), rhodonite (Si and Mn), jadeite (Na and Al), Ni metal (Ni) and celestite (Sr). Typical detection limits for elements, in ppm, are indicated in parentheses: Mg, Si and Ca (1000), Mn, Fe and Ni (3000) and Sr (2000). Beam currents were continuously monitored using a Faraday cup and analytical totals of 100 ± 2 wt% carbonate were obtained. The other dataset was obtained by electron probe microanalysis (EPMA) using a Cameca SX100 instrument at the University of Edinburgh. This electron probe was operated at two conditions: 15kV/2nA for Ca and Mg, and 15kV/40nA to measure Na, Al, Si, K, Mn, Fe, Ni, Co and Sr. Peak/background counting times were 20/10 to 40/20 secs, depending on the element being analysed. Standardisation used jadeite (Na), spinel (Mg, Al), wollastonite (Si), orthoclase (K), calcite (Ca), Mn metal (Mn), fayalite (Fe), celestite (Sr) and Ni metal (Ni). For all analyses the spot was defocused to 5 μm^2 in order to limit electron beam damage. Typical detection limits for elements, in ppm, are indicated in parentheses: Na (120), Mg (450), Al (110), Si (110), K (80), Ca (1500), Mn (550), Fe (300), Cr (210), Ni (280), Sr (310). Data from the two instruments are in excellent agreement with each other, and with results of previous analyses of QUE 93005 carbonates in de Leuw et al. (2010) (Fig. 1).

X-ray spectrum maps were acquired by EDX on the Zeiss SEM. As each pixel in these 1024×768 pixel maps contains information on X-ray intensities over energies up to 20 keV, the maps can be post-processed to reveal compositional information in a range of formats. Here greyscale element maps have been used to show variations over the scanned area in counts of one element, for example Ca K_α. The multielement maps were constructed using the INCA Cameo

programme whereby each pixel is assigned a colour according to the mean X-ray intensity over an energy range from 0.5 to 7.0 keV (i.e. encompassing energies from O K_α to Fe K_α inclusive). In these maps minerals rich in Mg and Si are orange to brown, Ca-rich minerals are green and Fe-rich minerals are blue. These colour blended maps have been overlain on the BSE image of the area scanned.

Carbonate mineral identification was undertaken by X-ray microanalysis together with Raman spectroscopy, the latter principally to distinguish aragonite from calcite. The Raman spectra were acquired using a Renishaw inVia Raman microscope with a 514 nm laser, and only 10% power was used in order to minimise sample damage. The laser was focused using a petrographic microscope equipped with a 100× objective. The spectra were accumulated in 30 increments with a measuring time of 2 sec. each. Calibration was made with respect to wavenumber using a Si standard and Raman spectra were processed (curve fitted) using the Reinshaw WIRE software.

2.4 Mn–Cr systematics

The crystallization ages of carbonates in primitive meteorites can be determined using the ^{53}Mn–^{53}Cr system (e.g. Endress et al., 1996; Brearley et al., 2001; de Leuw et al., 2009a, b; Tyra et al., 2010a; Petitat et al., 2011; Fujiya et al., 2012). Naturally occurring Mn has one stable isotope, ^{55}Mn, and eighteen radioisotopes. ^{53}Mn is the most stable of the radioisotopes and decays to ^{53}Cr with a half-life of 3.7 Ma. Hence, ^{53}Mn is extinct today but through the measurement of the excess of its daughter isotope, ^{53}Cr, the initial ^{53}Mn/^{55}Mn ratio at the time of carbonate crystallization can be determined. The excess of ^{53}Cr can be calculated since the natural terrestrial ^{53}Cr/^{52}Cr value is known to be 0.113458 (Papanastassiou 1986), where ^{52}Cr is the most abundant of the three stable Cr isotopes. The deviation from the natural terrestrial ratio is often expressed in parts per thousand (‰) as δ^{53}Cr. If there is a linear correlation between the measured ^{53}Cr/^{52}Cr and ^{55}Mn/^{52}Cr ratios, the slope of the line gives the initial ^{53}Mn/^{55}Mn ratio of the carbonate and the y-axis intercept gives the initial ^{53}Cr/^{52}Cr ratio.

The initial ^{53}Mn/^{55}Mn ratio of the carbonate can be compared with the ^{53}Mn/^{55}Mn ratio at the formation of the solar system to estimate a crystallisation age for the carbonate in the sample on the assumption of an initially uniform ^{53}Mn/^{55}Mn ratio throughout the solar system. However, the initial ^{53}Mn/^{55}Mn ratio is not so well defined. Most recently, Nyquist et al. (2009) estimated this ratio to be $9.1 \pm 1.7 \times 10^{-6}$ at 4568 (±1) Ma, and this value has been used here to calculate carbonate crystallization ages. To calculate the relative age (Δt) between two (^{53}Mn/^{55}Mn) ratios (e.g. between the formation of the solar system and the crystallisation of the carbonates in our sample), the standard equation for short lived radionuclides is:

$$\Delta t_{1\text{-}2} = \ln [(^{53}\text{Mn}/^{55}\text{Mn})_1 / (^{53}\text{Mn}/^{55}\text{Mn})_2] \times 1/\lambda \quad (1)$$

where λ is the decay constant of ^{53}Mn to ^{53}Cr and equals 1.87×10^{-7} yr^{-1} (Honda and Imamura, 1971).

The NanoSIMS 50L at the Carnegie Institutions of Washington was used for the *in situ* ^{53}Mn–^{53}Cr analyses by rastering a ~0.3 nA $^{16}O^-$ primary beam over a 5×5 μm^2 area on the polished

and C-coated sample. Each area was presputtered for 15 minutes prior to analysis. The masses ^{52}Cr, ^{53}Cr, and ^{55}Mn were monitored in multicollection mode using electron multipliers (EMs) at a mass resolution (~9000, as defined by Cameca) that was sufficient to resolve most likely isobaric interferences, but only partially resolve ^{52}CrH from ^{53}Cr and $^{54}CrH/^{54}FeH$ from ^{55}Mn. Hutcheon et al. (1998) showed that the hydride contributions at ^{53}Cr and ^{55}Mn are <1 ‰ and can be ignored. Certainly, no obvious hydride interferences were observed in scans across the ^{53}Cr and ^{55}Mn peaks during analysis of the hydrated matrix of QUE 93005. Nevertheless, ^{53}Cr and ^{55}Mn count rates were measured towards the low mass edges of the peaks where the hydride interferences would have been largely resolved.

San Carlos olivine has been the most commonly used standard for determining $^{55}Mn/^{52}Cr$ sensitivity factors. However, reported Mn/Cr ratios for San Carlos olivines exhibit a range of about a factor of two (e.g., Norman 1998; Ito and Ganguly, 2006; Hoppe et al. 2007; Spandler and O'Neill, 2010). Here, the standard used to determine the relative $^{55}Mn/^{52}Cr$ sensitivity factor was a synthetic diopside electron microprobe standard that was doped with 1.35 wt.% MnO and 1.28 wt.% Cr_2O_3. Six analyses of the diopside gave a $^{55}Mn/^{52}Cr$ relative sensitivity factor (measured/true), which includes the relative efficiencies of the two electron multipliers used to measure the two isotopes, of 1.08±0.04. The $\delta^{53}Cr$ values in the same diopside measurements exhibited a total range of 9 ‰ (1σ= 4 ‰). Fujiya et al. (2012) used a specially synthesised carbonate standard and obtained a sensitivity factor that is significantly lower (0.636-0.690) than for silicate standards (San Carlos olivine and synthetic diopside). If a lower sensitivity factor than determined on silicates ultimately proves to be more appropriate for carbonates, all previously determined carbonate ages will have to be adjusted. Here, we have chosen to use the sensitivity factor determined on our diopside standard to facilitate comparisons with earlier work.

To monitor temporal and spatial variations in the Cr isotope instrumental mass fractionation (IMF), matrix analyses were performed in the vicinity of each carbonate grain. The measured matrix Cr isotopic compositions did not vary systematically during a day's analyses, but did vary somewhat from day to day. The daily variation was from 6 ‰ to 20 ‰, i.e., of the order seen for the diopside standard despite the much greater physical and chemical heterogeneity of the matrix. The IMF correction for each day was calculated assuming that the matrix had the terrestrial $^{53}Cr/^{52}Cr$ ratio of 0.113459 (Papanastassiou, 1986). No attempt was made to make an internal mass fractionation correction using the other Cr isotopes because of potentially large isobaric interferences on them (^{50}Ti and ^{50}V on ^{50}Cr, and ^{54}Fe on ^{54}Cr). The range of isotopic compositions obtained on the diopside standard and matrix gives some idea of the ultimate precision of the analyses, but the variations are small compared to the $\delta^{53}Cr$ values measured in the carbonates (400-56,000 ‰).

Despite the presputtering, the carbonate $^{53}Cr/^{52}Cr$ and $^{55}Mn/^{52}Cr$ ratios always increased significantly (up to a factor of four in some cases) during the roughly hour-long analyses. These highly correlated changes were clearly the result of mixing of matrix-like and highly radiogenic components. Similar behavior has not been seen by us in the analyses of carbonates and fayalites in other meteorites. Despite the variations during the analyses, to avoid artifacts associated with the low count rates, the $^{53}Cr/^{52}Cr$ and $^{55}Mn/^{52}Cr$ ratios for each analysis were calculated by summing all

counts for each isotope, subtracting the EM background noise, and then applying the IMF and sensitivity factor corrections to the calculated ratios. The quoted uncertainties only account for counting statistics and the various corrections. No attempt was made to calculate the correlated errors associated with the change in the ratios during the analyses. However, because the correlated variations during the measurements were all along the isochron, the variations will not have compromised the initial $^{53}Mn/^{55}Mn$ ratio determination and the quoted errors will provide an accurate estimate of the expected scatter of the measured ratios about the isochron, and therefore the ultimate accuracy of the isochron fit.

The grains for Mn–Cr dating were selected carefully using BSE images and X-ray maps. An attempt was made to determine the crystallization ages of each of the four generations of carbonates in QUE 93005, but as described below ages were successfully obtained from the dolomite only. This was because the concentration of Mn in the calcite, and the Mn/Cr ratios in the breunnerite and the Ca-poor dolomite, were too low for dating using the Mn–Cr system. The dolomite grains analysed were all larger than 30 μm in diameter and their interiors were free of any potentially Cr-bearing inclusions (e.g. phyllosilicates).

3. RESULTS

3.1. Petrography and mineralogy of QUE 93005

SEM point counting shows that QUE 93005 contains 67.3 % matrix (including 4.1% fine-grained rims), 22.7 % partially or completely altered chondrules, 5.4% olivine/pyroxene grains isolated in the matrix, 3.8% carbonate, 0.7% sulphide and 0.1% Ca-phosphate. Four compositionally distinct carbonates are present, namely breunnerite, dolomite, Ca-poor dolomite and calcite. The Ca-carbonate was confirmed as calcite (rather than aragonite) by Raman spectroscopy. These minerals occur as monomineralic grains of breunnerite, calcite, and dolomite, are also intergrown as bimineralic dolomite–breunnerite, dolomite–calcite and very rarely breunnerite–Ca-poor dolomite grains, and can form polymineralic grains containing breunnerite, Ca-poor dolomite and calcite. These grains are described below in their inferred order of crystallisation.

3.2. Dolomite and dolomite–breunnerite grains

Dolomite occurs principally as monomineralic grains, but may also form bimineralic grains where intergrown with breunnerite or calcite. The monomineralic dolomite grains are typically ~50 μm in size, although the dolomite can also occur within hundreds of micrometer sized veins. All of the intact dolomite grains are rimmed by acicular Mg-Fe phyllosilicate crystals that are ~2.5-4.0 μm in length by ~0.1 μm in width (Figs. 2a and b). Those phyllosilicate crystals rimming any one dolomite grain are usually elongate in the same direction (Figs. 2a–c). Sulphide, mainly pentlandite, occurs as a selvage between sheaths of phyllosilicate crystals and as ~5 μm sized euhedral overgrowths on their terminations (Figs. 2a and b). The faces of these sulphide crystals may be parallel to cleavage planes of the enclosing dolomite (Fig. 2b). The mean composition of monomineralic dolomite grains obtained here is $Ca_{51.92}Mg_{35.75}Mn_{4.50}Fe_{7.81}Ni_{0.02}$ (n = 34), which is very close to the mean composition of $Ca_{52.14}Mg_{35.93}Mn_{4.66}Fe_{7.23}$ obtained from QUE 93005 dolomite by de Leuw et al. (2010), and the compositional ranges of the two datasets are very similar

(Fig. 1). A small proportion of the monomineralic dolomite grains have a central pore towards which zoned dolomite crystals present euhedral terminations, and the outermost parts of these crystals are enriched in Fe relative to the grain interiors.

The dolomite–breunnerite grains differ from monomineralic dolomite grains by the presence of a few micrometer sized crystals of breunnerite along one edge of the grain, and the interface between breunnerite and dolomite is invariably sharp and planar (Figs. 2c and d). These breunnerite crystals were too small for quantitative chemical analysis, but qualitative X-ray maps and spectra show that they may be zoned with respect to Mg and Fe (Fig. 2e). In all of the dolomite–breunnerite grains examined the dolomite is compositionally zoned, as revealed by CL imaging (Fig. 2d) with the non-luminescent zone being enriched in Fe relative to the luminescent region. Zone boundaries lie parallel to dolomite cleavages and to the planar interface between breunnerite and dolomite, indicating that the breunnerite has formed on a former dolomite crystal face (Fig. 2d). The pattern of zoning in the CL image reveals clearly the direction of crystal growth and so demonstrates that dolomite predates breunnerite (Fig. 2d). The phyllosilicate-sulphide rims to some dolomite and dolomite–breunnerite grains are absent so that the broken interior of the grain is juxtaposed with the meteorite matrix (Fig. 2e). Fragments of these rims may lie nearby the parent grain (Fig. 2e) or occur isolated in the meteorite matrix (Fig. 2f).

3.3. Breunnerite and breunnerite–Ca-poor dolomite grains

Monomineralic breunnerite grains are equant, ~40-100 μm in size, and composed of ~10-20 μm sized crystals (Fig. 3). One of the breunnerite grains also contained a rectilinear inclusion of Ca-poor dolomite, and this carbonate generation is described in more detail below (Fig. 3b). Inclusions of acicular ~10 μm long phyllosilicates occur throughout the breunnerite grains and are commonly coated by films of sulphide (Fig. 3a). Owing to the abundance of these inclusions all chemical analyses contained considerable quantities of phyllosilicate-derived Mg, Si and Fe so that breunnerite mineral compositions were unobtainable from these grains by EDX or EPMA, regardless of the spot size used.

3.4. Polymineralic grains

The polymineralic grains are equant, ~50-300 μm in size, and contain breunnerite, Ca-poor dolomite and calcite (Figs. 4 and 5). Breunnerite occurs at or close to grain margins and has abundant phyllosilicate inclusions that are often encrusted by sulphide (Figs. 5a and b). In one of the polymineralic grains is a meshwork of pentlandite needles is intergrown with breunnerite, which demonstrates that the pentlandite has replaced breunnerite (Fig. 4a). Analyses of breunnerite contain 0.8 to 8.7 wt% SiO_2, which comes from phyllosilicate inclusions, and the plots in Fig. 6 show that these inclusions have the effect of lowering concentrations of Fe in the most Si-rich analyses, but have little effect on Mg or Ca values. The fourteen analyses with lowest Si concentrations (here taken as less than 2 wt% SiO_2) yield a mean breunnerite composition of $Ca_{3.21}Mg_{59.12}Mn_{2.52}Fe_{35.10}Sr_{0.04}$. The breunnerite layer is often compositionally zoned with parts closest to grain centres being enriched in Mn and Fe (Figs. 4d and e).

Ca-poor dolomite is typically intergrown with breunnerite and may: (i) form a narrow (typically ~3-6 μm, but exceptionally 15 μm thick) overgrowth on breunnerite substrates (Figs. 4a and 5a–c), (ii) fill rectilinear patches within breunnerite (Fig. 4c), (iii) cross-cut breunnerite as veins (Fig. 4c), and (iv) replace breunnerite at grain margins (Fig. 4). Phyllosilicate inclusions are more abundant in Ca-poor dolomite than breunnerite (Fig. 5d) and are often intergrown with sulphide. X-ray analyses of phyllosilicate-bearing but sulphide-free areas of Ca-poor dolomite yielded 0.7 to 7.8 wt% SiO_2 (n = 26) and with increasing Si the Mg and Fe concentrations also increase and Ca values decrease (Fig. 6). The three analyses with less than 2 wt% SiO_2 yield a mean composition for the Ca-poor dolomite of $Ca_{43.36}Mg_{43.66}Mn_{1.43}Fe_{11.51}Ni_{0.02}Sr_{0.01}$. The interface of Ca-poor dolomite with calcite in the centre of polymineralic grains is curving and decorated with sub-micrometer sized pores (Figs. 5a–c).

The calcite is free of micropores and mineral inclusions (Figs. 4 and 5); phyllosilicate crystals within Ca-poor dolomite are truncated at its interface with calcite (Fig. 5d). The calcite comprises single crystals that are zoned in both CL images and Mn concentrations, and the zoning patterns are consistent with crystal growth from the interface with Ca-poor dolomite towards the grain centre. The mean composition of this calcite is $Ca_{97.69}Mg_{0.57}Mn_{0.85}Fe_{0.89}Ni_{0.01}Sr_{0.00}$ (n = 22). In common with the monomineralic dolomite grains and the bimineralic dolomite-breunnerite grains, parts of the rims to polymineralic grains are missing so that Ca-poor dolomite or calcite is in contact with the meteorite matrix (Figs. 4a, 4c, 5c).

3.5. Calcite grains and dolomite–calcite grains

SEM point counting shows that monomineralic calcite grains comprise 0.7 vol. % of the sample. They are tens of micrometers in size and characteristically contain euhedral sulphides (Fig. 7a), which de Leuw et al. (2010) identified as pentlandite, pyrrhotite and intermediate sulphides. Many of the calcite grains are aggregates of crystals that have irregular boundaries and significantly different orientations (Figs. 7a and b). The ratio of dolomite to calcite in the bimineralic grains ranges from those dominated by calcite with small dolomite inclusions (Figs. 7c and d) to grains with roughly equal proportions of the two carbonates. The calcite-dominated bimineralic grains can be up to several hundred micrometers in size, are equant to elongate in shape and characteristically have rounded margins (Fig. 7c). Inclusions of dolomite (Fig. 7d) can occur anywhere within the grain, whereas the equant sulphides are concentrated around their margins (Fig. 7c). As illustrated in Figs. 8a and b, several calcite-rich bimineralic grains occur in a cluster along with monomineralic dolomite grains. The dolomite grains are petrographically identical to those found elsewhere in the thin section, whereas the bimineralic grains are slightly larger, with rounded margins, and contain inclusions of dolomite together with sulphides and micropores (Figs. 8a and b). The dolomite grains have their characteristic phyllosilicate-sulphide rims, whereas rims are absent from the associated bimineralic grains (Fig. 8a). EBSD shows that all of the dolomite and dolomite–calcite grains in this cluster have the same crystallographic orientation (Fig. 8c). Elsewhere in the thin section are bimineralic grains that have approximately equal proportions of calcite and dolomite and the boundaries between the two minerals may be planar and oriented parallel to dolomite cleavages (Figs. 8d). In the large bimineralic vein in Figs. 8e and 7f the dolomite parts have planar interfaces

with the meteorite matrix together with phyllosilicate-sulphide rims, whereas the calcite-rich parts are sulphide-free and have rounded contacts with the meteorite matrix.

Calcite, dolomite and Fe,Ni sulphide occur in narrow veins that cross-cut the fine-grained rims to aqueously altered chondrules (Figs. 9a, b). Some of these veins contain both dolomite and calcite (Figs 9c and d) whereas others have calcite only (Figs. 9e and f). The veins are ~5-10 μm in width, have wedge-shaped ends (Figs, 9e, f), rarely penetrate into the surrounding meteorite matrix, and most are oriented with their long axes approximately normal to the chondrule-rim interface (Figs. 9b and f). In Fig. 9b the veins occur on opposite sides of the chondrule but are orientated with their long axes in a similar direction (i.e. NE-SW relative to the image).

Calcite of all grain types is relatively pure, with an average composition of $Ca_{99.48}Mg_{0.13}Fe_{0.33}Mn_{0.05}Ni_{0.01}Sr_{0.01}$ (n = 29), which is close to analyses of QUE 93005 calcite grains in de Leuw et al. (2010) of $Ca_{99.04}Mg_{0.25}Fe_{0.43}Mn_{0.22}$.

3.6. Carbonate grains used for Mn–Cr age determinations

We successfully analysed dolomite in five monomineralic grains and four bimineralic grains (Table 1). In three of the bimineralic grains, the dolomite is intergrown with calcite, and in one it is intergrown with breunnerite. Two of the dolomite grains and one of the dolomite-calcite grains occur together in the cluster shown in Figs. 10a and b. The $^{53}Cr/^{52}Cr$ vs. $^{55}Mn/^{52}Cr$ ratios of all the measured dolomites and an extra point, which represents the average matrix analysis, are plotted in Fig. 10. All points lie within error of a single isochron. The value of the initial $^{53}Mn/^{55}Mn$ ratio given by the slope of the best-fit line in Fig. 10 is $4.37\pm0.19\times10^{-6}$ (2σ), MSWD=1.20. Despite the abundance of phyllosilicate inclusions in the breunnerite and Ca-poor dolomite, an attempt was made to analyse them via ion imaging, whereby images of the sample are acquired rather than just recording the total number of ions from the analyzed area. With simultaneous images of Si-, Mn- and Cr-isotopes, the Si-rich areas can in principle be removed and the counts in the rest of the imaged carbonate can be summed. However, the regions with the highest Mn/Cr ratios in the imaged areas had values of only ~70, which is far below the ~10,000 that is needed for measurable ^{53}Cr excesses to be observed. This implies that the breunnerite and Ca-poor dolomite contain Cr, or the inclusions are Cr-bearing and could not be avoided during analysis, regardless of spot size.

4. DISCUSSION

4.1. Mechanisms of carbonate mineralisation

The presence of QUE 93005 carbonates in veins is inconsistent with their crystallisation in the solar nebula. The evidence for extensive variations of solution compositions, to produce the bimineralic and polymineralic grains, together with the Mn–Cr ages of dolomite, also shows that these minerals could not have been produced by Antarctic weathering and so we therefore conclude that they formed by parent body aqueous processes. In the Introduction three mechanisms of parent body carbonate mineralisation were hypothesised, namely cementation, dissolution-precipitation and replacement, and below each of the mechanisms has been tested, principally using evidence from the bimineralic and polymineralic grains.

4.1.1. Evidence for cementation

The dolomite-breunnerite grains together with all three carbonates in the polymineralic grains are typically compositionally zoned (e.g. Fig. 2d). Such zoning is ubiquitous in calcite cements within terrestrial rocks where it demonstrates that the crystals grew into open pore space (e.g. Lee and Harwood, 1989). As calcite from CM2s is also commonly zoned (e.g. Brearley, 1998; Brearley and Hutcheon, 2000, 2002; Lee and Ellen, 2008) it is likewise interpreted to have formed by cementation of open pores. The morphology of carbonate grains suggests that these pores may have been equidimensional although the degree to which the matrix has been compacted around the carbonate grains is difficult to assess. The larger veins are most likely to have formed by occlusion of fracture pores (Fig. 8e), and one context where it is clear how these fractures formed is with regards to the calcite–dolomite–sulphide veins that cross-cut fine-grained chondrule rims (Fig. 9). These veins are inferred to have formed by cementation of open fractures. As most veins lie at a high angle to chondrule-rim interfaces, the fine-grained rims are most likely to have fractured in response to expansion of the rimmed chondrule, and the wedge shape tips of the veins is consistent with fracture dilation propagating outwards from the chondrule edge. The chondrules could have expanded during hydration of their silicates and glass, and this is indeed the outcome if the major ions (Mg, Si and Fe) are immobile. For example, the replacement of forsterite and enstatite by chrysotile, as expressed in equation (2) (Guo and Eiler, 2007), is accompanied by a 44% increase in volume:

$$Mg_2SiO_4 + MgSiO_3 + 2H_2O \rightarrow Mg_3Si_2O_5(OH)_4 \quad (2)$$

Veins that cross-cut chondrule rims have also been described by Krot et al. (2000) from MAC 88107 (an ungrouped carbonaceous chondrite with CM affinities) and by Tomeoka and Ohnishi (2010) from Mokoia (CV3). The MAC 88107 veins are composed of magnetite, olivine and hedenbergite whereas in Mokoia they contain olivine, magnetite and Fe-Ni sulphides. Krot et al. (2000) concluded that the veins in MAC 88107 formed by filling of fractures produced by rim breakage following oxidation and expansion of opaque nodules in the outermost parts of chondrules, whereas Tomeoka and Ohnishi (2010) interpreted the abrupt truncation of Mokoia veins at the outer edge of the rims to indicate that they formed in a precursor parent body region.

In common with MAC 88107, the veins in QUE 93005 chondrule rims are inferred to have formed by expansion of the chondrules *in situ* and during aqueous alteration, although this is likely to have taken place after hydration of the matrix (Rubin et al., 2007). The termination of veins at the rim-matrix interface is most likely due to differences in the mechanical properties of the rims and matrix as a consequence of contrasts in grain size. As these veins typically occur on opposite sides of the chondrule, the fractures may have developed whilst the chondrule and rim were under an anisotropic confining pressure. For example for the rimmed chondrule in Fig. 9 the axis of compression may have been oriented NE-SW, which would have allowed fracture dilation on a SE-NW axis. Given the concentration of Ca in outer parts of the chondrule pseudomorphs (Fig. 9b) it is most likely that the Ca for calcite and dolomite was sourced from within the chondrule and was transported towards the matrix through the open fractures. This is consistent with the suggestion by

Brearley (2006b) that Ca for Ca-carbonates and Ca-phosphates in meteorite matrices was derived from chondrule mesostases, although Ca-rich glass may have also been present in the matrix. As the chondrule mesostasis was most likely aqueously altered before olivine, whose alteration led to the expansion, the Ca may have been sourced from recrystallisation of earlier generations of secondary minerals.

4.1.2. Evidence for dissolution-precipitation and replacement

There is also good evidence in QUE 93005 that calcite has formed at the expense of dolomite, and that Ca-poor dolomite has formed at the expense of breunnerite. The replacement of dolomite by calcite is termed 'dedolomitisation' if the reaction is true replacement, or calcitisation if calcite crystallises within pores formed by dissolution of dolomite (Lee and Harwood, 1989; Nader et al., 2008). The principal evidence for dedolomitisation is the presence of corroded relicts of dolomite within calcite-rich bimineralic grains (Fig. 7d) and the fine-scale crystallographically controlled intergrowths of dolomite with calcite (e.g. Fig. 8d). Further information on the nature of the replacement reaction is provided by the cluster of dolomite grains and calcite-rich bimineralic grains in Figs. 8a and b. As these grains share an identical crystallographic orientation the original dolomite grains must have been interconnected, and those crystallographic orientations were retained by topotactic replacement of dolomite by calcite. Many of the monomineralic calcite grains probably also formed by dedolomitisation because they are commonly polycrystalline and their constituent crystals have very different orientations that suggests piecemeal replacement of the precursor dolomite. The monomineralic calcite grains and the calcite-rich bimineralic grains are characteristically micropore-rich and have rounded margins, and so are petrographically distinct from the precursor dolomite crystals that are micropore-free and have straighter edges. These contrasts suggest that replacement was not quite pseudomorphic so that some of the calcite extended into the matrix to give the grains rounded profiles. de Leuw et al. (2010) invoked late-stage dedolomitisation to account for some of the differences in carbonate mineralogy between the CMs that they had studied, and QUE 93005 provides the petrographic confirmation that this process was operative in at least one parent body region. The chemistry of the dedolomitisation reaction is discussed below.

There is no evidence for replacement of breunnerite by calcite, which may be due to its low concentrations of Ca, or just its scarcity of breunnerite within the meteorite, but Ca-poor dolomite has formed at the expense of breunnerite. In some cases this was by replacement, as demonstrated by the inclusions of breunnerite within Ca-poor dolomite that rims some polymineralic grains. Where Ca-poor dolomite occurs in intra-breunnerite pores (Figs 3b and 4c) there must have been a longer time gap between dissolution of breunnerite and crystallisation of Ca-poor dolomite (i.e. dissolution-precipitation). The corroded interface between Ca-poor dolomite and calcite was the product of another later episode of carbonate dissolution. Although there is good evidence for pseudomorphic replacement of chondrule olivine and pyroxene by calcite in CM2s including Cold Bokkeveld (Greenwood et al., 1994), this process is unlikely to have been significant in QUE 93005 because carbonates are rare in chondrules and where they have formed by replacement it is of earlier carbonates.

QUE 93005 therefore contains evidence for all three of the mechanisms of carbonate mineralisation that were hypothesised in the Introduction (i.e. cementation, dissolution-precipitation and replacement), although pore-filling cementation was the volumetrically most important process. This conclusion contrasts with the suggestion by de Leuw et al. (2009b) that carbonates 're-equilibrated continuously' during alteration of the most highly hydrated CM2s including QUE 93005 (i.e. as fluid compositions changed existing carbonates dissolved and new ones precipitated). Results of the present study suggest that there was only minor re-equilibration by dissolution-precipitation or replacement in QUE 93005, but simply continuing cementation of a relatively porous and permeable region of its parent body in step with changing pore fluid compositions. As the first carbonate to crystallise was dolomite (rather than calcite in the less highly altered CM2s), it is possible that carbonates started to form in QUE 93005 later relative to alteration of the matrix and chondrules so that pore fluids had significantly greater Mg/Ca and Fe/Ca values. Potential sequences of carbonate crystallisation within QUE 93005 and other CMs are discussed below.

4.2. Relative chronology of mineralisation

The relative chronology of carbonate mineralisation in QUE 93005 is revealed by petrographic relationships between different generations of carbonates within the bimineralic and polymineralic grains. As discussed above, these intergrowths formed predominantly by multiphase cementation, although dissolution-precipitation and replacement were also operative, and all three mechanisms require substantial changes in solution compositions. The sequence of mineralisation as inferred from bimineralic and polymineralic grains is described below and also illustrated in Figure 11.

4.2.1. Mineralisation sequence inferred from the bimineralic grains

For the dolomite–breunnerite grains, CL imaging shows that dolomite crystallised first, near completely filling the pore space, prior to breunnerite overgrowing crystal terminations (Fig. 2d). Some of the dolomite grains subsequently underwent partial to complete dedolomitisation to form the dolomite–calcite grains (e.g. Fig. 8d) and the monomineralic calcite grains respectively (e.g. Fig. 7c). Together the two types of bimineralic grains show that the sequence of mineralisation was dolomite, breunnerite then calcite (Fig. 11). In the single breunnerite–Ca-poor dolomite grain found petrographic relationships suggest that the Ca-poor dolomite has filled a pore on the edge of the breunnerite grain with a crystallographically controlled shape (Fig. 3b). This relationship suggests that Ca-poor dolomite postdated breunnerite dissolution, and the same relationships are seen within the polymineralic grain in Figure 4 (discussed below).

4.2.2. Mineralisation sequence inferred from the polymineralic grains

The concentric layering of the polymineralic grains shows that breunnerite crystallised first at the pore margin, to be followed by Ca-poor dolomite with calcite filling the pore centre (Fig. 4a). As the Ca-poor dolomite occasionally occurs as rectilinear inclusions within breunnerite it is interpreted to have crystallised following etching of the breunnerite to make pores with crystallographically controlled shapes, although in other parts of these grains the Ca-poor dolomite

has replaced the breunnerite. At their interface with calcite the Ca-poor dolomite crystals have rounded and microporous edges instead of euhedral terminations (Figs. 5b, c), which indicates that they were partially dissolved prior to calcite precipitation. The calcite crystallised as a cement to fill any remaining pore space, as evidenced by its commonplace CL and trace element zoning. The sequence of mineralisation in the polymineralic grains was therefore breunnerite, Ca-poor dolomite, then calcite (Fig. 11).

4.2.3. Overall mineralisation sequence

There is no evidence for the relative ages of the bimineralic and polymineralic grains. However the simplest model is that dolomite formed first and where it did not completely fill the pore space it was overgrown by breunnerite. The breunnerite also filled small pores elsewhere in the matrix to make monomineralic breunnerite grains, and crystallised around the margins of larger pores to form the outermost layer of polymineralic grains. After a hiatus during which time the breunnerite was etched to leave pores with crystallographically controlled shapes, Ca-poor dolomite grew within intra-breunnerite pores and on etched breunnerite terminations because at this time breunnerite was the only carbonate mineral lining partially filled pores. The final phase saw crystallisation of calcite, which filled pore space remaining in the polymineral grains and replaced dolomite (Fig. 11). Compositional differences between the replacive and pore-filling calcite may however suggest that it crystallised from fluids of different chemical compositions, and possibly at different times.

An alternative scenario is that breunnerite then Ca-poor dolomite crystallised before dolomite, and after a brief second period of breunnerite crystallisation on dolomite substrates the calcite crystallised as a cement within the polymineralic grains and also replaced dolomite. In this scenario the evolution of pore fluid chemistry is largely unidirectional (i.e. yielding carbonates with a progressively greater Ca/Mg ratio), but it is difficult to account for why dolomite did not overgrow Ca-poor dolomite in the polymineralic grains. This scenario also requires a second phase of breunnerite crystallisation to form the overgrowths on dolomite crystal terminations.

A third possibility is that dolomite, and breunnerite together with Ca-poor dolomite, crystallised in different parts of the QUE 93005 parent body at approximately the same time owing to significant spatial variations of fluid compositions. However, the occurrence of these minerals throughout the sample argues against such compartmentalisation of the aqueous system. We conclude that the simplest and, therefore, most likely sequence of mineralisation was dolomite, breunnerite, Ca-poor dolomite then calcite (Fig. 11).

4.3. Crystallisation of phyllosilicates and sulphides associated with carbonates

Phyllosilicate and sulphide inclusions within carbonates can help to refine the relative chronologies outlined above. As the orientations of the acicular phyllosilicate crystals within dolomite are controlled by the dolomite crystal structure (Figs 2a, c), the phyllosilicates are clearly replacive of preexisting dolomite. The phyllosilicates must also have formed after the breunnerite and Ca-poor dolomite that they have replaced. Significant differences in the degree of replacement of dolomite by phyllosilicates, compared to breunnerite and Ca-poor dolomite, may simply be due to the greater

concentrations of Mg and Fe in breunnerite and Ca-poor dolomite. By the same reasoning, the absence of phyllosilicate inclusions within calcite could be due to its paucity of Mg and Fe, but the truncation of inclusions at the etched interface of Ca-poor dolomite with calcite (Fig. 5d) suggests that the phyllosilicates crystallised before dissolution of Ca-poor dolomite and calcite cementation. Replacement of carbonates by phyllosilicates is infrequently reported, although Changela and Bridges (2011) described siderite that had been replaced by phyllosilicates in the nakhlite meteorite Lafayette. The timing of carbonate mineralisation relative to aqueous alteration of anhydrous matrix silicates is difficult to determine with certainty. The presence of calcite and dolomite within fractures cross-cutting fine-grained chondrule rims shows that the carbonates had formed after some hydration and expansion of chondrule glass and/or silicates, yet the replacement of carbonates by phyllosilicates suggests that towards the end of carbonate mineralisation solutions still had substantial concentrations of Mg, Si and Fe. We therefore propose that the carbonates crystallised during early stages of hydration of the meteorite matrix.

As the habit of the sulphide crystals that rim dolomite grains is also dictated by the dolomite crystal structure (Fig. 2b), the sulphides must postdate dolomite, and this conclusion is in agreement with the findings of de Leuw et al. (2010). The sulphides also occur between phyllosilicate crystals and have overgrown their terminations, and so some or all of them must have formed after the phyllosilicates, and so after breunnerite and Ca-poor dolomite that the phyllosilicates have replaced. The distinctive sulphide rims occur only on dolomite crystals and so it is likely that an interaction of sulphide-precipitating solutions with dolomite was a determinant of that style of sulphide crystallisation. By contrast the calcite grains have been replaced by coarser equant sulphides, and this difference may be explained by the calcite being more soluble than dolomite during replacement so that its crystal structure exerted less of a control on the habit of the sulphides. The timing of phyllosilicate and sulphide precipitation relative to carbonate mineralisation is summarised in Fig. 11.

4.4. Loss of carbonate grain rims

The edges of many of the carbonate grains have been lost, and shards of grain edges together with their phyllosilicate-sulphide rims are isolated within the meteorite matrix, thus demonstrating that parts of QUE 93005 have experienced considerable mechanical deformation. Grain breakage must have postdated replacement of dolomite by sulphides because fragments of dolomite grain rims have sulphides on only one side (i.e. the original grain margin) (Fig. 2f). One possible mechanism for loss of carbonate grain edges is by shearing along planes within the matrix (i.e. faults) accompanying impacts (i.e. ‘regolith gardening’). Carbonate grains in the matrices of other CM2s, including Murray, are cross-cut by small displacement faults (Lee and Ellen, 2008), and extensive mechanical damage to QUE 93005 carbonate grains can be reconciled with the preservation of intact rimmed chondrules (Fig. 9a), dolomite veins (Fig. 8e) and carbonate grain clusters (Fig. 8a) if the effects of shock were highly heterogeneous. An alternative mechanism is suggested by the focusing of breakage on carbonate grain margins, which is suggestive of a process of abrasion of the grains by rotation within the matrix. This rotation may have taken place before or during compaction, but another possibility is that abrasion accompanied fluidisation of the matrix by gas or

vapour, and grain abrasion during fluidisation has been described from terrestrial pyroclastic deposits (Gravina et al., 2004). With regard to QUE 93005 the gas may have been CH_4 generated during serpentinisation (Guo and Eiler 2007), H_2 from oxidation of Fe (Wilson et al., 1999; Alexander et al., 2010) or the CO/CO_2 that contributed to carbonate crystallisation. Water vapour could also have been generated from deeper in the parent body by depressurisation following removal of overburden by impacts or by catastrophic overpressure (Wilson et al., 1999). It might be expected that the damaged carbonate grains would be concentrated in parts of the matrix through which the gas/vapour escaped, but as their distribution within the sample was not determined this possibility remains untested. The presence of dish structures within a dark inclusion from the Vigarano (CV3) meteorite (Tomeoka and Kojima, 1998) confirms that fluidisation was active in parent body environments.

4.5. Carbonate ages

All the analyzed dolomite grains, be they monomineralic, bimineralic or present in a cluster, fall on the same isochron meaning that they all formed over a relatively short time interval. The initial ($^{53}Mn/^{55}Mn$) ratio is $4.37\times10^{-6}\pm1.9\times10^{-7}$ (2σ), MSWD=1.20 (Fig. 10). This value is within error of previous Mn–Cr analyses of dolomite in QUE 93005, $4.1 \pm 1.2 \times 10^{-6}$ (2σ), MSWD = 3.3 (de Leuw et al., 2009b), but here with an order of magnitude better precision. Using the ($^{53}Mn/^{55}Mn$) ratio for the beginning of the solar system as derived by Nyquist et al. (2009) and the standard equation for short-lived radionuclides (Honda and Imamura, 1971), the crystallisation age of the dolomite in our sample is 3.93 ± 0.23 Ma (with the error derived only from the construction of the isochron). The crystallisation age is 3.93 ± 1.7 Ma if the error also includes the uncertainty of the initial $^{53}Mn/^{55}Mn$ value. Our petrographic results demonstrate that dolomite was the first carbonate to crystallise (or at least the oldest that is preserved), and was followed by breunnerite, Ca-poor dolomite and calcite in addition to phyllosilicates and sulphides. Thus the ~4 Ma age marks the start of the record of carbonate mineralisation in QUE 93005 (Fig. 11), which may or may not have been synchronous with the onset of aqueous activity.

Our age constraints on QUE 93005 carbonate mineralisation would be consistent with a later onset of aqueous alteration than previous models have suggested (e.g. de Leuw et al., 2009b), although with the caveat that the time interval between liquid water first being present in the QUE 93005 parent body region and dolomite crystallisation is unknown. Nonetheless this ssuggestion of a late onset of alteration is consistent with recent work by Fujiya et al. (2012). They used nanoSIMS to analyse calcite in Murchison (CM2.5) and Y791198 (CM2.4) and dolomite in ALH83100 and Sayama (both CM2.1) and for a standard employed synthetic calcite doped with Mn and Cr rather than the more usual silicates (e.g. olivine or diopside) used in the present study and by previous workers (e.g. Hoppe et al., 2007; de Leuw et al., 2009b; Petitat et al., 2011). With the caveat that ages obtained using the different standards are not directly comparable, Fujiya et al. (2012) found that carbonates from the four meteorites have an identical age of $4563.4\ ^{+0.4}_{-0.5}$ Ma (i.e. ~4.8 Ma after CAI formation). By combining these age data with models of parent body thermal histories Fujiya et al. (2012) concluded that the parent body or bodies of the four meteorites studied accreted at least 3 Ma after CAIs.

4.6. Evolution of fluid compositions during aqueous alteration

The mineralisation history of carbonate grains is consistent throughout the QUE 93005 thin section, even down to the etching of Ca-poor dolomite prior to calcite cementation. Hence, water/rock (*w/r*) ratios must have been sufficient so that solutes could move and homogeneise over millimeter- to centimeter-scales by aqueous diffusion and over timescales shorter than those of carbonate crystal growth. Given that most of the QUE 93005 carbonate grains have occluded pore spaces as cements, the minimum effective porosity of the rock during carbonate mineralisation must equal the volume of carbonate now present (i.e. 3.8 vol. %). This suggestion of relatively high *w/r* ratios during carbonate crystallisation is supported by the remarkable compositional homogeneity of dolomite (Fig. 1) and its occurrence within hundreds of micrometer-sized veins and interconnected grain clusters. As dolomite is the first carbonate to have crystallised, it would be expected to have filled the largest and most highly interconnected pores. If, by contrast, the aqueous solutions had been physically and chemically isolated, for example by a low permeability matrix (Bland et al., 2009), they are more likely to have crystallised carbonates whose compositions and/or mineralisation sequences would be far more spatially variable (i.e. reflecting local differences in solution chemistry).

Of the three carbonate minerals that have been previously described from the CM2s, calcite occurs in all meteorites, aragonite is found in the relatively unaltered ones, including Murray and Murchison (Barber, 1981; Lee and Ellen, 2008; Sofe et al., 2011), whereas dolomite is limited to the most highly aqueously altered samples (Zolensky et al., 1997; Rubin et al., 2007). This pattern suggests that as alteration progressed Ca-carbonate was followed by dolomite, probably reflecting increasing fluid Mg/Ca accompanying hydration of ferromagnesian silicates. However, petrographic evidence for replacement of Ca-carbonate by dolomite and/or precipitation of dolomite on Ca-carbonate substrates has been absent. QUE 930005 is the first CM2 within which the relative chronology of carbonate crystallisation can be determined unambiguously, and surprisingly it reveals a sequence of mineralisation that is opposite to the one predicted (i.e. dolomite together with Ca-poor dolomite and breunnerite predate calcite). Even if aragonite or calcite did crystallise in QUE 93005 very early, as previous models for the CM2s would predict, but was subsequently dissolved or completely replaced by dolomite and/or phyllosilicates, any model still needs to account for why a second generation of calcite has formed after the Mg-Ca-Fe carbonates. The alternative is to suggest that QUE 93005 is atypical of the CM2s, but that is unsatisfactory because it fits readily into CM2 alteration sequences as defined by various chemical and mineralogical parameters (e.g. Rubin et al., 2007; de Leuw et al., 2010; Howard et al., 2011).

An insight into the nature of the late-stage calcite-precipitating fluids may come from consideration of the solution chemistry required for dedolomitisation. On Earth this reaction is mediated by low Mg/Ca solutions that for example have been produced by dissolution of Ca-sulphates (Lee and Harwood, 1989). The reaction for pseudomorphic (i.e. volume-for-volume) replacement of one mole of QUE 93005 dolomite by calcite, may be written as follows (modified from Ayora et al., 1998):

$$Ca_{1.038}Mg_{0.715}Mn_{0.090}Fe_{0.156}(CO_3)_2 + 0.258H^+ + 0.695Ca^{2+} = 1.742Ca_{0.994}Mg_{0.001}Mn_{0.001}Fe_{0.003}CO_3 + 0.713Mg^{2+} + 0.089Mn^{2+} + 0.150Fe^{2+} + 0.258HCO_3^- \quad (3)$$

Thus, for each mole of QUE 93005 dolomite replaced, 0.695 moles of Ca needs to be imported into the grain, and 0.713, 0.089 and 0.150 moles of Mg, Mn and Fe respectively are lost from the grain. If all of the 0.7 vol. % of monomineralic calcite grains in QUE 93005 are assumed to have formed by dedolomitisation, every 1 cm^3 of meteorite contains 0.007 cm^3 of calcitised dolomite, which would require 3.61 mg of Ca in solution. Assuming a *w/r* ratio of 1 and complete removal of Ca from solution during the reaction, the fluids would need to have a minimum Ca concentration of 3600 mg/l. A more realistic *w/r* ratio of 0.2 gives a minimum Ca concentration of 18,000 mg/l, which shows that these late-stage solutions were Ca-rich. They would also need to have had low Mg/Ca and Fe/Ca concentrations in order to crystallise the relatively compositionally pure calcite. Mg and Fe could been removed from solution relative to Ca by crystallisation of Mg-Fe phyllosilicates. The presence of Ca-rich solutions relatively late in the alteration history of QUE 93005 is unexpected given that the sources of Ca, such as mesostasis glass and clinopyroxene, would be expected to liberate Ca to solution relatively early (as discussed above with reference to calcite veins in fine-grained chondrule rims). Ca may however have been enriched in the pore fluids as a by-product of crystallisation of the Ca-poor matrix phyllosilicates. A further possibility is that Ca in solution was introduced from another parent body region, which follows the suggestion by Zolensky et al. (1997) that the abundance of Ca-carbonates in highly altered CM2 meteorites reflected the concentration of Ca in a manner similar to the formation of caliche in terrestrial soils. The difficulty with invoking such a process is that it requires the movement of solutes by advection over length scales considerably greater than individual meteorites, which contradicts empirical models of carbonaceous chondrite alteration that envisage fluid movement over millimeters at most (Bland et al., 2009). This possibility of fluid movement is discussed further below.

4.7. Conditions of aqueous alteration of QUE 93005 and the other CM2s

QUE 93005 differs from most CM2s in that tochilinite is absent and instead Fe-Ni sulphides are widespread within carbonate grains and elsewhere in the meteorite matrix. As the CM1 meteorites also lack tochilinite its absence from QUE 93005 is probably because it has been recrystallised as aqueous alteration has progressed. Thus QUE 93005 has evolved along a path similar to the CM1s but the duration of aqueous activity must have been significantly shorter owing to loss of water, rather than its consumption *in situ*. One way in which water could have been lost is by vapourisation, for example following depressurisation accompanying removal of overburden by an impact. As discussed above, rapid loss of water vapour through an unconsolidated parent body could in turn have led to fluidisation of the matrix and abrasion of the carbonate grains.

The conditions under which QUE 93005 was aqueously altered can be explored further using the chemistry and mineralogy of carbonate minerals in other carbonaceous chondrite groups. The compositional range of QUE 93005 carbonates is greater than in any other CM2 previously described, although its dolomite has a composition that is typical of the CM2s (Fig. 12). CM1 carbonates differ considerably in composition between meteorites. ALH 88045 and MET 01070

contain Ca-carbonate only (Zolensky et al., 1997; de Leuw et al., 2010), whereas dolomite and other Mg-, Mn- and Fe-rich carbonates are present in EET 83334 (Zolensky et al., 1997) and the paired meteorites ALH 84034, 84049 and 84051 (Brearley and Hutcheon, 2000; Tyra et al., 2009, 2010a). The CM1 SCO 06043 also contains both dolomite and calcite with good evidence for formation of the calcite by dedolmitisation (Lindgren et al., 2012). In common with QUE 93005, the dolomite in both ALH 84051 and SCO 06034 occurs in millimeter to tens of millimeter long veins, although in ALH 84051 they are 10s of millimeters in length (Mark Tyra, *personal communication* 2012). Overall the CM1 carbonates have a broad compositional range that overlaps with most of the dolomite and Ca-poor dolomite in QUE 93005 and includes breunnerite, although those analyses are richer in Mg than QUE 93005 breunnerite (Fig. 12).

The CR carbonaceous chondrites are typically dominated by Ca-carbonates (Weisberg et al., 1993), but Tyra et al. (2011b) have described grains in the CR1 meteorite GRO 95577 that are comprised of an intergrowth of calcite, dolomite and siderite. These carbonates have also been replaced by sulphide (pyrrhotite) and serpentine intergrown with pentlandite. The GRO 95577 grains are, therefore, almost identical in mineralogy to the QUE 93005 polymineralic grains. As regards to relative timing of mineralisation in GRO 95577, O isotope data suggest that in contrast to QUE 93005 calcite predated the Fe-rich carbonate (siderite) (Tyra et al., 2011a), but in common with QUE 93005 petrographic results indicate that phyllosilicates crystallised after the Fe-rich carbonates (Tyra et al., 2011b). The CI meteorites contain four carbonate minerals, which in order of abundance are dolomite, breunnerite, calcite and siderite (Fredriksson and Kerridge 1988; Johnson and Prinz, 1993; Riciputi et al., 1994; Endress and Bischoff, 1996; Lee and Nicholson, 2009). The CI dolomite compositions overlap the range of Ca-poor dolomite in QUE 93005, but only partly overlap the range of its dolomite (Fig. 12). QUE 93005 breunnerite also generally has higher concentrations of Fe that CI breunnerites, although a few analyses in Endress and Bischoff (1996) do coincide with the QUE 93005 range. One grain of siderite has been described from the CI meteorite Ivuna ($Ca_{15.4}Mg_{37.8}Fe_{46.8}Mn_{0.0}$). This compares with the most Fe-rich breunnerite from QUE 93005 whose composition of $Ca_{5.7}Mg_{47.7}Fe_{43.4}Mn_{3.0}$ lies close to the breunnerite-siderite boundary. Tagish Lake (ungrouped C2) contains Ca-carbonates (aragonite and calcite), calcian dolomite and siderite (Zolensky et al., 2002; Nakamura et al., 2003; Isawa et al., 2010) and so also has a similar carbonate mineralogical diversity as QUE 93005. In the carbonate-poor lithology of Tagish Lake Ca-carbonate is the most abundant carbonate followed by dolomite and rare siderite. By contrast the carbonate-rich lithology contains abundant Ca-carbonate grains that are rimmed and cross-cut by siderite (Zolensky et al., 2002). The crystallisation sequence of Ca-carbonate followed by Fe-Mg carbonate in Tagish Lake is therefore opposite to the sequence inferred from the QUE 93005 polymineralic grains.

These comparisons suggest an affinity between QUE 93005 and the CM1, CR1 and CI meteorites. The very strong similarity in mineral assemblages of polymineralic grains in QUE 93005 and the CR1 GRO 95577 imply that during carbonate mineralisation solution temperatures and/or solution chemistry, pH and Eh may have been comparable between the two meteorites. Suggested crystallisation temperatures for carbonates in the CM2s Cold Bokkeveld, Murray and Murchison from clumped isotope thermometry are 20-71 ºC (Guo and Eiler, 2007), which is lower

than temperatures suggested for CR aqueous alteration of <150 ºC (Zolensky et al., 1993) to 250-300 ºC (Weisberg and Huber 2007), although the very primitive nature of organic matter in the CRs would argue for temperatures lower than those previously published (see Alexander et al., 2010).

The exceptionally wide range of carbonate mineral compositions in QUE 93005 is evidence for extensive changes in solution compositions, which are hard to reconcile with models for CM aqueous alteration that invoke essentially static solutions. In particular the solutions that mediated late-stage dedolomitisation must have been very different in composition from those that precipitated the dolomite and breunnerite. Although the provenance of these fluids is unknown, the evidence for dedolomitisation in the CM1 SCO 06043 (Lindgren et al., 2012) suggests that late-stage Ca-rich solutions were associated with the same parent body regions that experienced the most extensive matrix hydration. With the finding by Tyra *et al.* (2012) of two isotopically distinct generations of calcite in a CM2, there is now a body of evidence for aqueous processing of the CM carbonaceous chondrites by multiple pulses of chemically and isotopically distinct solutions that needs to be reconciled with models for the thermal, aqueous and structural evolution of parent bodies.

5. CONCLUSIONS

QUE 93005 records a multiphase history of carbonate mineralisation. Dolomite forming first in the largest and best connected pores, then was followed by breunnerite, Ca-poor dolomite and calcite, and precipitation of Ca-poor dolomite and calcite was preceded by a phase of dissolution. The dolomite crystallised at 3.93 ± 0.23 Ma after solar system formation, and this date is likely to be near to the start of the aqueous alteration history of the parent body region and prior to at least some of the matrix phyllosilicates and sulphides, but during or after hydration and subsequent expansion of chondrules. At the time of chondrule hydration, the region of the parent body from where QUE 93005 was derived was under an aniostropic confining pressure so that fractures that developed in the fine-grained rims as chondrules expanded opened only in low-stress orientations. The degree of aqueous alteration of QUE 93005 shows that it is a highly hydrated CM2, and this classification is consistent with its carbonate mineralogy, which is comparable to the CM1s, CI1s and the one CR1. The diversity of carbonate minerals in QUE 93005 suggest that it was aqueously altered by several fluid generations of contrasting composition and, most likely different provenance, and although all CM2 must by definition have lost water prior to completion of aqueous alteration, QUE 93005 provides some evidence that this may have been due to late-stage matrix fluidisation.

ACKNOWLEDGEMENTS

We thank Peter Chung for assistance with the SEM and Chris Hayward (University of Edinburgh) for help with the electron probe analyses. We are grateful to NASA for loan of the QUE 93005 thin section and to Kieren Howard, Mark Tyra and Mike Zolensky for very thorough and helpful reviews. This research was funded by grants from the UK STFC.

REFERENCES

Alexander C. M. O'D., Newsone S. D., Fogel M. L., Nittler L. R., Busemann H. and Cody G. D. (2010) Deuterium enrichments in chondritic macromolecular material – implications for the origin and evolution of organics, water and asteroids. *Geochim. Cosmochim. Acta* **74**, 4417–4437.

Ayora C., Taberner C., Saaltink M. W. and Carrera J. (1998) The genesis of dedolomites: a discussion based on reactive transport modelling. *Journal of Hydrology* **209**, 346–365.

Barber D. J. (1981) Matrix phyllosilicates and associated minerals in C2M carbonaceous chondrites. *Geochim. Cosmochim. Acta* **45**, 945–970.

Barber D. J. (1985) Phyllosilicates and other layer structured materials in stony meteorites. *Clay Mineral.* **20**, 415–454.

Benedix G. K., Leshin L. A., Farquhar J., Jackson T. and Thiemens M. H. (2003) carbonates in CM2 chondrites: Constraints on alteration conditions from oxygen isotopic compositions and petrographic observations. *Geochim. Cosmochim. Acta* **67**, 1577–1588.

Bland P. A., Jackson M. D, Coker R. F., Cohen B. A., Webber B. W., Lee M. R., Duffy C. M., Chater R. J., Ardakani M. G., McPhail D. S., McComb D. W. and Benedix, G. K. (2009) Why aqueous alteration in asteroids was isochemical: High porosity ≠ high permeability. *Earth Planet. Sci. Lett.* **287**, 559–568.

Brearley A. J. (1998) Carbonates in CM carbonaceous chondrites: Complex zoning revealed by high resolution cathodoluminescence studies. *Lunar Planet. Sci.* **29**. Lunar Planet. Inst., Houston. #1246 (abstr.).

Brearley A. J. (2006a) The action of water. In Meteorites and the Early Solar System II. D.S. Lauretta, H.Y. McSween, Jr., editors.

Brearley A.J. (2006b) The role of microchemical environments in the alteration of CM carbonaceous chondrites. *Lunar Planet. Sci.* **37**. Lunar Planet. Inst., Houston. #2074 (abstr.).

Brearley A. J. and Hutcheon I. D. (2000) Carbonates in the CM1 chondrite ALH8034: Mineral chemistry, zoning and Mn-Cr systematics. *Lunar Planet. Sci.* **31**. Lunar Planet. Inst., Houston. #1407 (abstr.).

Brearley A. J. and Hutcheon I. D. (2002) Carbonates in the Y791198 CM2 chondrite: zoning and Mn-Cr systematics (abstract). *Meteorit. Planet. Sci.* **37**, A23.

Brearley A. J. Saxton J. M. Lyon I. C. and Turner G. (1999) Carbonates in the Murchison CM chondrite: CL characteristics and oxygen isotopic compositions. *Lunar Planet. Sci.* **30**. Lunar Planet. Inst., Houston. #1301 (abstr.).

Brearley A. J. Hutcheon I. D. and Browning L. (2001) Compositional zoning and Mn-Cr systematics in carbonates from the Y791198 CM2 carbonaceous chondrite. *Lunar Planet. Sci.* **32**. Lunar Planet. Inst., Houston. #1458 (abstr.).

Brearley A. J. Weber P. and Hutcheon I. D. (2006) Trace element zoning in CM chondrite carbonates: insights from compositional mapping using nanosims. *Meteorit. Planet. Sci.* **41**, abstract no. 5365.

Bunch T. E. and Chang S. (1980) Carbonaceous chondrites: II. Carbonaceous chondrite phyllosilicates and light element geochemistry as indicators of parent body processes and surface conditions. *Geochim. Cosmochim. Acta* **44**, 1543–1577.

Changela H. G. and Bridges J. C. (2011) Alteration assemblages in nakhlites: Variation with depth on Mars. *Meteorit. Planet. Sci.* **45**, 1847–1867.

de Leuw S., Rubin A. E. and Wasson, J. T. (2006a) Carbonates and associated sulphide rims in CM chondrites: Complex formational histories. *Lunar Planet. Sci.* **39**. Lunar Planet. Inst., Houston. #1179 (abstr.).

de Leuw S., Rubin A. E. and Wasson J. T. (2006b) Manganese-rich phases in CM chondrites: Mn-Cr systematics of carbonates and silicates. *Meteorit. Planet. Sci.* **41**, abstract no. 5168.

de Leuw S. Rubin A. E. and Wasson J. T. (2007) Manganese-rich alteration phases in the CM chondrites of different petrographic subtypes: Implications for the timing of aqueous alteration. *Lunar Planet. Sci.* **38**. Lunar Planet. Inst., Houston. #1361 (abstr.).

de Leuw S., Rubin A. E., Schmidt A. K. and Wasson, J. T. (2009a) Mn-Cr systematics for the CM2.1 chondrite QUE 93005 and ALH 83100: Implications for the timing of asteroidal alteration. *Lunar Planet. Sci.* **40**. Lunar Planet. Inst., Houston. #1794 (abstr.).

de Leuw S., Rubin A. E., Schmidt A. K. and Wasson, J. T. (2009b) ^{53}Mn-^{53}Cr systematics of carbonates in CM chondrites: Implications for the timing and duration of aqueous alteration. *Geochim. Cosmochim. Acta* **73**, 7433–7442.

de Leuw S., Rubin A. E., Schmidt A. K. and Wasson J. T. (2010) Carbonates in CM chondrites: Complex formational histories and comparison to carbonates in CI chondrites. *Meteorit. Planet. Sci.* **45**, 513–530.

Endress M., Zinner E. and Bischoff A. (1996) Early aqueous activity on primitive meteorite parent bodies. *Nature* **379**, 701–703.

Fredriksson K. and Kerridge J. F. (1988) Carbonates and sulfates in CI chondrites – formation by aqueous activity on the parent body. *Meteorit. Planet. Sci.* **23**, 35–44.

Fuchs L. H., Olsen E. and Jensen K. J. (1973) Mineralogy, mineral chemistry and composition of the Murchison (C2) meteorite. *Smithson. Contrib. Earth Sci.* **10**, 1–39.

Fujiya W., Sugiura N., Hotta H., Ichimura K., and Sano Y. (2012) Evidence for the late formation of hydrous asteroids from young meteoritic carbonates. *Nature Communications* **3**, 627. Doi: 10.1038/ncomms1635 (2012).

Grady M. M. Wright I. P. Swart P. K. and Pillinger C. T. (1988) The carbon and oxygen isotopic composition of meteoritic carbonates. *Geochim. Cosmochim. Acta* **52**, 2855–2866.

Gravina T., Lirer L., Marzocchella A., Petrosino P. and Salatino P. (2004) Fluidisation and attrition of pyroclastic granular solids. *J. Volcano. Geotherm. Res.* **138**, 27–42.

Greenwood R. C., Lee M. R., Hutchison R. and Barber D. J. (1994) Formation and alteration of CAIs in Cold Bokkeveld (CM2). *Geochim. Cosmochim. Acta* **58**, 1913–1935.

Grossman J. N. and Score R. (1996) The meteoritical bulletin, No. 79, 1996 July. *Meteorit. Planet. Sci.* **31**, A161–A174.

Guo W. and Eiler J. M. (2007) Temperatures of aqueous alteration and evidence for methane generation on the parent bodies of the CM chondrites. *Geochim. Cosmochim. Acta* **71**, 5565–5575.

Hoppe P., MacDougall D., Lugmair G.W. (2007) High spatial resolution ion microprobe measurements refine chronology of carbonate formation in Orgueil. *Meteorit. Planet. Sci.* **42**, 1309–1320.

Howard K. T., Benedix G. K., Bland P. A. and Cressey G. (2009) Modal mineralogy of CM2 chondrites by PSD-XRD: Part 1. Total phyllosilicate abundance and the degree of aqueous alteration. *Geochim. Cosmochim. Acta* **73**, 4576–4589.

Howard K. T., Benedix G. K., Bland P. A. and Cressey G. (2011) Modal mineralogy of CM chondrites by X-ray diffraction (PSD-XRD): Part 2. Degree, nature and settings of aqueous alteration. *Geochim. Cosmochim. Acta* **75**, 2735–2751.

Hutcheon I. D., Krot A. N., Keil K., Phinney D. L. and Scott E. D. R. (1998) ^{53}Mn-^{53}Cr dating of fayalite formation in the CV3 chondrite Mokoia: Evidence for asteroidal alteration. *Science* **282**, 1865–1867.

Honda M., Imamura M. (1971) Half-life of ^{53}Mn. Physical Review C4, 1182-1188.

Isawa M. R. M., Flemming R. L., McCausland P. J. A., Southam G., Moser D. E. and Barker I. R. (2010) Multi-ttechnique investigation reveals new mineral, chemical and textural heterogeneity in the Tagish Lake C2 chondrite. *Planet. Space Sci.* **58**, 1347-1364.

Ito M. and Ganguly J. (2006) Diffusion kinetics of Cr in olivine and ^{53}Mn-^{53}Cr thermochronology of early solar system objects. *Geochim. Cosmochim. Acta* 70, 799-809.

Johnson C. A. and Prinz M. (1993) carbonate compositions in CM and CI chondrites, and implications for aqueous alteration. *Geochim. Cosmochim. Acta* **57**, 2843–2852.

Krot A. N., Brearley A. J., Petaev M. I., Kallemeyn G. W., Sears D. W. G., Benoit P. H., Hutcheon I. D., Zolensky M. E. and Keil K. (2000) Evidence for low-temperature growth of fayalite and hedenbergite in MacAlpine Hills 88107, an ungrouped carbonaceous chondrite related to the CM-CO clan. *Meteorit. Planet. Sci.* **35**, 1365–1386.

Lee M. R. and Harwood G. M. (1989) Dolomite calcitisation and cement zonation related to uplift of the Raisby Formation (Zechstein carbonate), northeast England. *Sedimentary Geology* **65**, 285–305.

Lee M. R. and Ellen R. (2008) Aragonite in the Murray (CM2) carbonaceous chondrite: implications for parent body compaction and aqueous alteration. *Meteorit. Planet. Sci.* **43**, 1219–1231.

Lee M. R. and Nicholson K. (2009) Ca-carbonate in the Orgueil (CI) carbonaceous chondrite: Mineralogy, microstructure and implications for parent body history. *Earth Planet. Sci. Lett.* **280**, 268–275.

Lindgren P., Lee, M. R., Sofe, M. R. and Burchell M. J. (2011) Microstructure of calcite in the CM2 carbonaceous chondrite LON 94101: Implications for deformation history during and/or after aqueous alteration. *Earth Planet. Sci. Lett.* **306**, 289–298.

Lindgren P., Lee M. R. and Sofe M. (2012) Evidence for multiple fluid pulses in the CM1 carbonaceous chondrite parent body. *Lunar Planet. Sci.* **40**. Lunar Planet. Inst., Houston. #1949(abstr.).

McSween H. Y. (1979) Alteration in CM carbonaceous chondrites inferred from modal and chemical variations in matrix. *Geochim. Cosmochim. Acta* **43**, 1761–1770.

Nakamura T. Noguchi T. Zolensky M. E. and Tanaka M. (2003) Mineralogy and noble-gas signatures of the carbonate-rich lithology of the Tagish Lake carbonaceous chondrite: evidence for an accretionary breccia. *Earth Planet. Sci. Lett.* **207**, 83–101.

Nader, F. H., Swennen, R. and Keppens, E. (2008) Calcitisation/dedolomitisation of Jurassic dolostones (Lebanon): results from petrographic and sequential geochemical analysis. *Sedimentology* **55**, 1467–1485.

Norman M. D. (1998) Melting and metasomatism in the continental lithosphere: laser ablation ICPMS analysis of minerals in spinel lherzolites from eastern Australia. *Contrib. Mineral. Petrol.* **130**, 240-255.

Nyquist L. E., Kleine T., Shih C.-Y. and Reese Y. D. (2009) The distribution of short-lived radioisotopes in the early solar system and the chronology of asteroid accretion, differentiation and secondary mineralisation. *Geochim. Cosmochim. Acta* **73**, 5115–5136.

Papanastassiou D. A. (1986) Chromium isotope anomalies in the Allende meteorite. *Astrophysical Journal* **308**, L27–L30.

Petitat M., Marrocchi Y., McKeegan K. D., Mostefaoui S., Meibom A., Zolensky M. E. and Gounelle M. (2011) ^{53}Mn-^{53}Cr ages of Kaidun carbonates. *Meteorit. Planet. Sci.* **46**, 275–283.

Riciputi L. R. McSween H. Y. Jr. Johnson C. A. and Prinz M. (1994) Minor and trace element concentratsions in carbonates of carbonaceous chondrites, and implications for compositions of co-existing fluids. *Geochim. Cosmochim. Acta* **58**, 1343–1351.

Rubin A. E., Trigo-Rodriguez J. M., Huber H. and Wasson J. T. (2007) Progressive aqueous alteration of CM carbonaceous chondrites. *Geochim. Cosmochim. Acta* **71**, 2361–2382.

Sofe M. R., Lee M. R. and Lindgren P. (2011) Aragonite in the CM carbonaceous chondrites: A proxy for the magnitude of aqueous alteration. *Meteorit. Planet. Sci.* **46**, abstract no. 5250.

Spandler C. and O'Neill H. St. C. (2010) Diffusion and partition coefficients of minor and trace elements in San Carlos olivine at 1,300 °C with some geochemical implications. *Contrib. Mineral. Petrol.* **159**, 791–818.

Tomeoka K. and Kojima, T. (1998) Arcuate band texture in a dark inclusion from the Vigarano CV3 chondrite: Possible evidence for early sedimentary processes. *Meteorit. Planet. Sci.* **33**, 519–525.

Tomeoka K. and Buseck P. R. (1985) Indicators of aqueous alteration in CM carbonaceous chondrites: Microtextures of a layered mineral containing Fe, S, O, and Ni. *Geochim. Cosmochim. Acta* **49**, 2149–2163.

Tomeoka K. and Ohnishi I. (2010) Indicators of parent-body processes: Hydrated chondrules and fine-grained rims in the Mokoia CV3 carbonaceous chondrite. *Geochim. Cosmochim. Acta* **74**, 4438–4453.

Tyra M. A., Brearley A. J., Hutcheon I. D., Ramon E., Matzel J. and Weber, P. (2009) Carbonate Formation timescales vary between CM1 chondrites ALH84051 and ALH84034. *Lunar Planet. Sci.* **40**. Lunar Planet. Inst., Houston. #2474 (abstr.).

Tyra M. A., Matzel J., Brearley A. J. and Hutcheon I. D. (2010a) Variability in carbonate petrography and NanoSims $^{53}Mn/^{53}Cr$ systematics in paired CM1 chondrites ALH 84051, ALH 84049, and ALH 84034. *Lunar Planet. Sci.* **41**. Lunar Planet. Inst., Houston. #2687 (abstr.).

Tyra M. A., Brearley A. J., Matzel J. and Hutcheon I. D. (2010b) Types and timescales of secondary carbonates in the CR1 chondrite GRO 95577. *Lunar Planet. Sci.* **41**. Lunar Planet. Inst., Houston. #2614 (abstr.).

Tyra M. A., Brearley A. J. and Guan Y. (2011a) Oxygen isotopic composition of secondary carbonates in CR1 chondrite GRO 95577. *Lunar Planet. Sci.* **42**. Lunar Planet. Inst., Houston. #1639 (abstr.).

Tyra M. A., Le Guillou C. and Brearley A. J. (2011b) Deciphering the history of carbonates and associated minerals during secondary alteration within CR1 GRO 95577. *Meteorit. Planet. Sci.* **46**, abstract no. 5446.

Tyra M. A., Farquhar J. Guan Y. and Leshin L. A. (2012) An oxygen isotope dichotomy in CM2 chondritic carbonates—A SIMS approach. *Geochim. Cosmochim. Acta* **77**, 383–395.

Velbel M. A., Tonui E. K. and Zolensky M. E. (2005) Aqueous alteration in QUE93005 (CM2): Different alteration scales for Antarctic and non-Antarctic CM chondrites? *Meteorit. Planet. Sci.* **40**, abstract no. 5191.

Weisberg M. K., Prinz M., Clayton R. N. and Mayeda T. K. (1993) The CR (Renazzo-type) carbonaceous chondrite group and its implications.*Geochim. Cosmochim. Acta* **57**, 1567–1586.

Weisberg, M. K. and Huber, H. (2007) The GRO 95577 CR1 chondrite and hydration of the CR parent body. *Meteorit. Planet. Sci.* **42**, 1495–1503.

Wilson L., Keil K., Browning L. B., Krot A. N. and Bourcier W. (1999) Early aqueous alteration, explosive disruption, and reprocessing of asteroids. *Meteorit. Planet. Sci.* **34**, 541–557.

Zolensky M. E., Barrett R. and Browning L. (1993) Mineralogy and composition of matrix and chondrule rims in carbonaceous chondrites. *Geochim. Cosmochim. Acta* **57**, 3123–3148.

Zolensky M. E., Mittlefehldt D. W., Lipschutz M. E., Wang M.-S.,Clayton R. N., Mayeda T. K., Grady M. N., Pillinger C. and Barber D. J. (1997) CM chondrites exhibit the complete petrologic range from type 2 to 1. *Geochim. Cosmochim. Acta* **61**, 5099–5115.

Zolensky M. E., Nakamura K., Gounelle M., Mikouchi T., Kasama T., Tachikawa O. and Tonui E. (2002) Mineralogy of Tagish Lake: An ungrouped type 2 carbonaceous chondrite. *Meteorit. Planet. Sci.* **37**, 737-761.

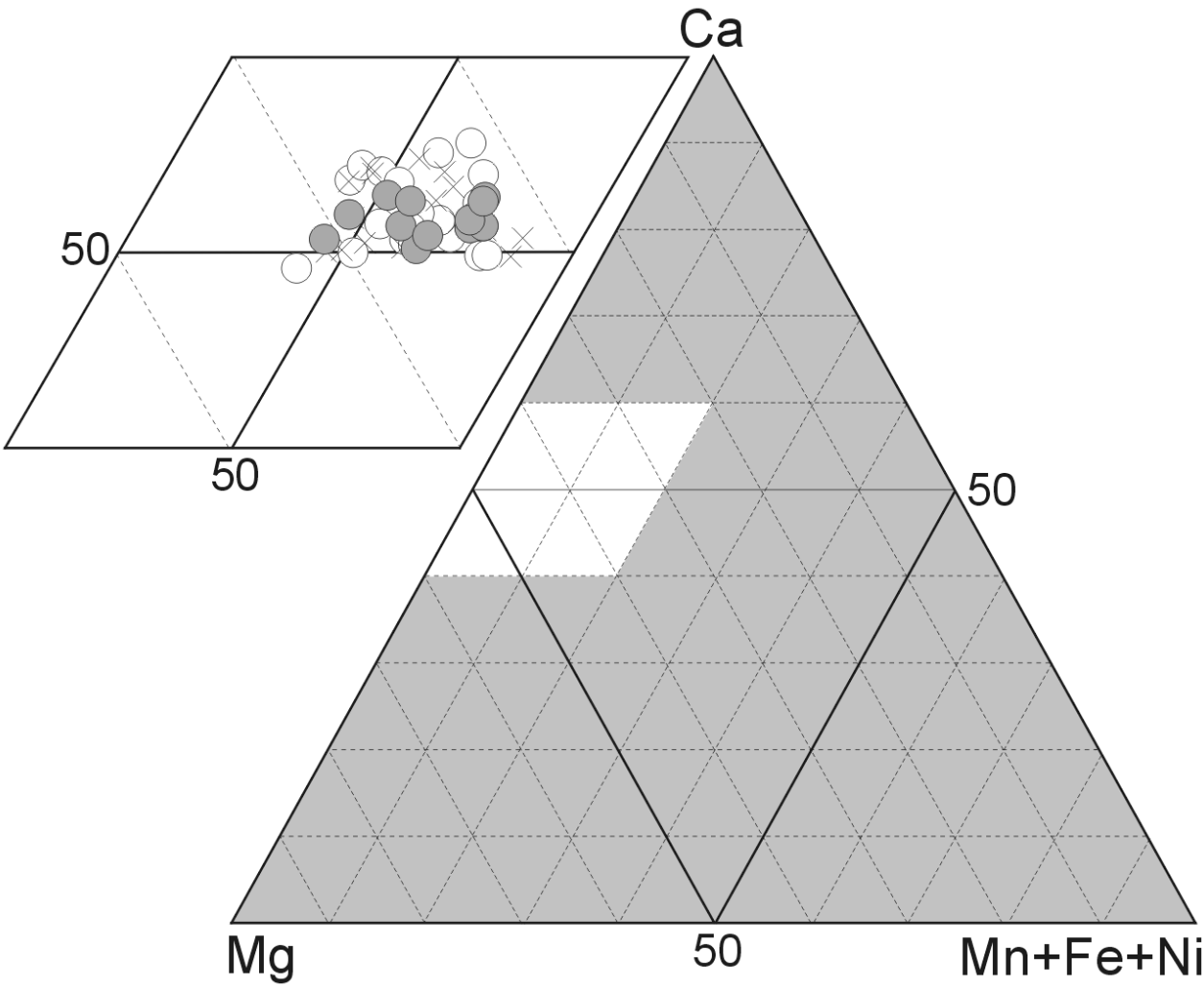

Figure 1. Comparison of the chemical compositions (mole%) of QUE 93005 dolomite grains determined in the present study by EDX (open circles, n = 22) and EPMA (grey circles, n = 12) with compositions for QUE 93005 dolomite in de Leuw et al. (2010) (crosses, n = 16).

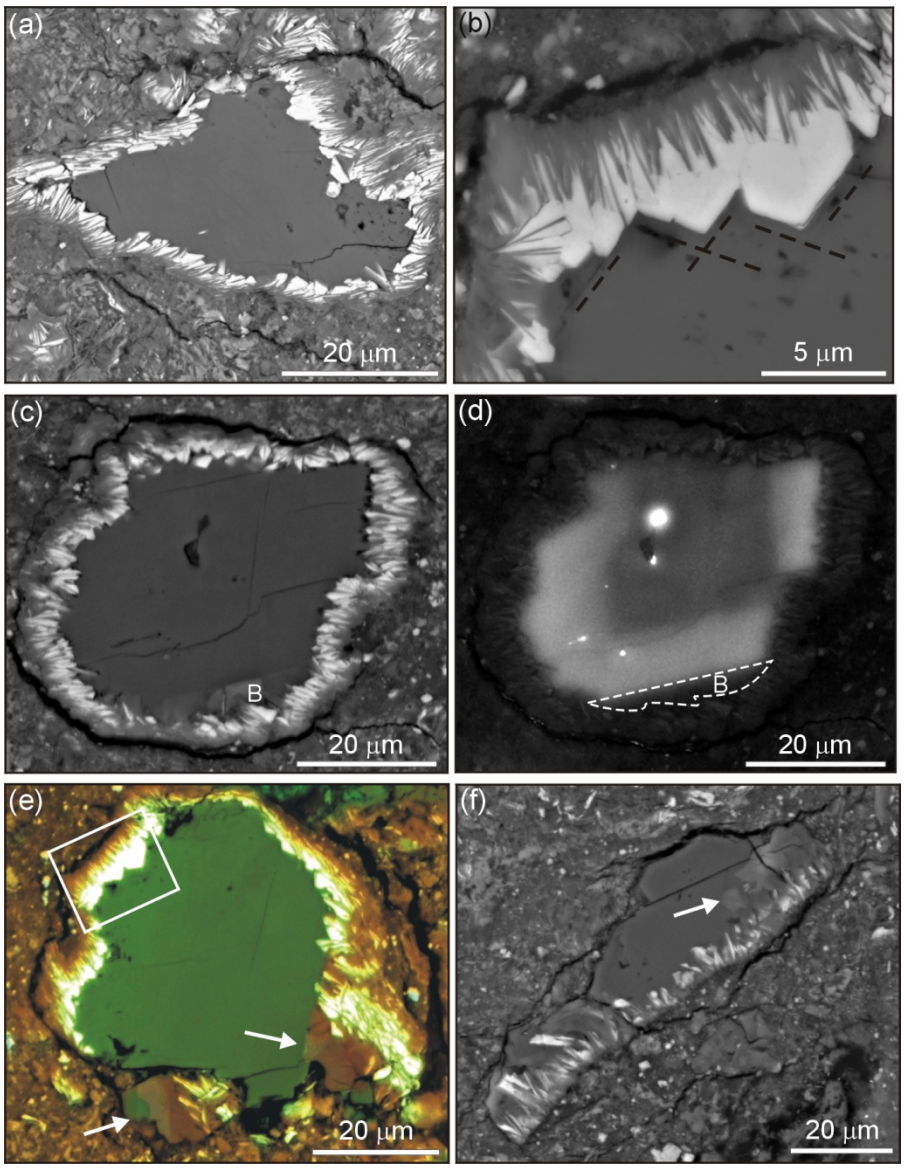

Figure 2. Dolomite and dolomite–breunnerite grains. (a) BSE image of a dolomite grain with a phyllosilicate–sulphide rim. Most of the phyllosilicate crystals are elongate roughly horizontally regardless of the orientation of the dolomite grain margin. (b) BSE image of a dolomite grain margin showing that sulphides (white) have overgrown the terminations of acicular phyllosilicate crystals. The sulphides have euhedral terminations consistent with the having grown as micrometer-sized single crystals, and these crystal faces lie parallel to the traces of cleavages planes in other parts of the same dolomite grain (indicated by dashed black lines). (c) BSE image of a dolomite grain with breunnerite (B) at its bottom edge. The interface of dolomite with breunnerite is sharp and planar, and oriented parallel to the ENE-WSW set of dolomite cleavages. On the left and right hand sides of the grain the constituents of the phyllosilicate-sulphide rim are elongate parallel to the same cleavage set. (d) SEM-CL image of (c) showing that the dolomite is zoned and zone boundaries are parallel to dolomite cleavages and to the dolomite-breunnerite interface. Zoning shows that the dolomite crystal nucleated at the top edge of the grain and grew downwards. The

breunnerite (B) is non-luminescent and so its location is delineated by a dashed white line. (e) Multielement X-ray map of a grain that is composed predominantly of dolomite (dark green) with two areas of breunnerite (arrowed, red-brown). Note that the breunnerite is zoned from light to darker red-brown and that one of the breunnerite crystals is contained within a broken piece of the grain margin. The boxed area is shown enlarged in (b). (f) Fragment of the rim to a dolomite–breunnerite grain that is isolated within the meteorite matrix. The breunnerite crystals are arrowed, and notably the phyllosilicate–sulphide rim occurs only on one side of the grain fragment.

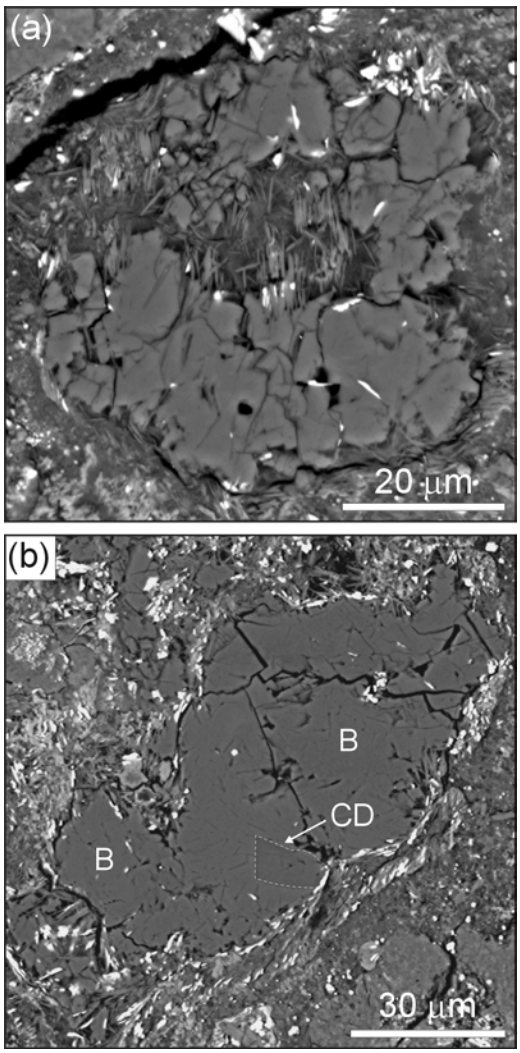

Figure 3. (a) BSE image of a polycrystalline breunnerite grain that has abundant inclusions of fibrous phyllosilicates. Most of these fibres are hard to distinguish from the breunnerite except where they are rimmed by sulphides (white). The phyllosilicates in the grain centre could have formed by replacement of breunnerite or they may have grown within an area unfilled by breunnerite. (b) BSE image of the only bimineralic breunnerite–Ca-poor dolomite grain found. Most of the breunnerite (B) contains fibrous phyllosilicate inclusions. The dashed white line outlines a small rectilinear area of Ca-poor dolomite (CD).

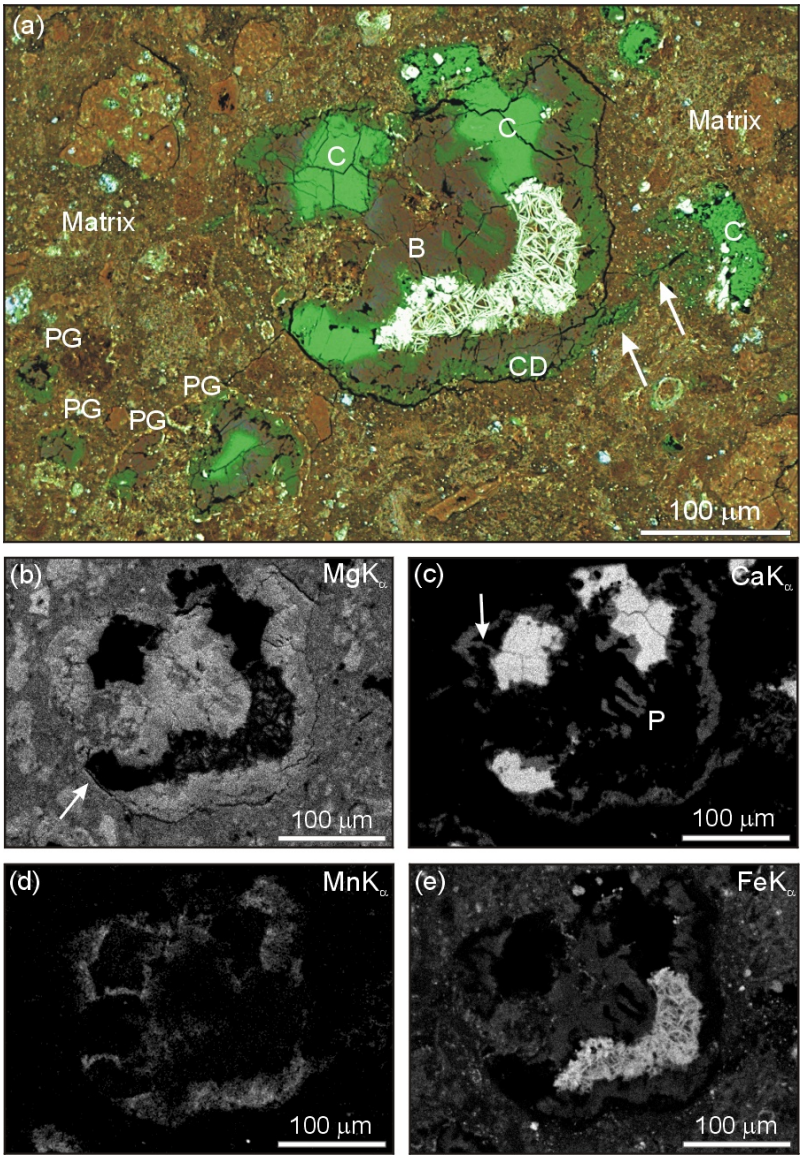

Figure 4. (a) Multielement X-ray map of a polymineralic grain and adjacent carbonates. The phyllosilicate rich matrix is brown, breunnerite (B) is red-brown, Ca-poor dolomite (CD) is dark green and calcite (C) is lime green. The breunnerite around the edge of the largest polymineralic grain (centre of the image) has been extensively replaced by Ca-poor dolomite, and a selvage of Ca-poor dolomite also occurs between the breunnerite and calcite. The breunnerite has additionally been partly replaced by a meshwork of pentlandite needles (white). The matrix in the lower left of the image contains four smaller polymineralic grains (PG), three of which are dominated by breunnerite and Ca-poor dolomite and the largest contains all three carbonates. An irregular vein of calcite (arrowed) extends from the right hand corner of the largest polymineral grain towards a calcite grain (C). (b) Mg K_α X-ray map of the largest polymineralic grain in (a). Breunnerite is light grey, Ca-poor dolomite is medium grey and calcite is black. Note that along its lower left edge the grain has been broken (arrowed) so that calcite is juxtaposed with the meteorite matrix. (c) Ca K_α

X-ray map highlighting calcite (white) and Ca-poor dolomite (grey). The Ca-poor dolomite cross-cuts breunnerite as a vein (arrowed) and has also occluded angular intra-breunnerite pores (P). (d) Mn K_α X-ray map highlighting zoning in the breunnerite. (e) Fe K_α X-ray map showing that the breunnerite (grey) is also zoned with respect to Fe.

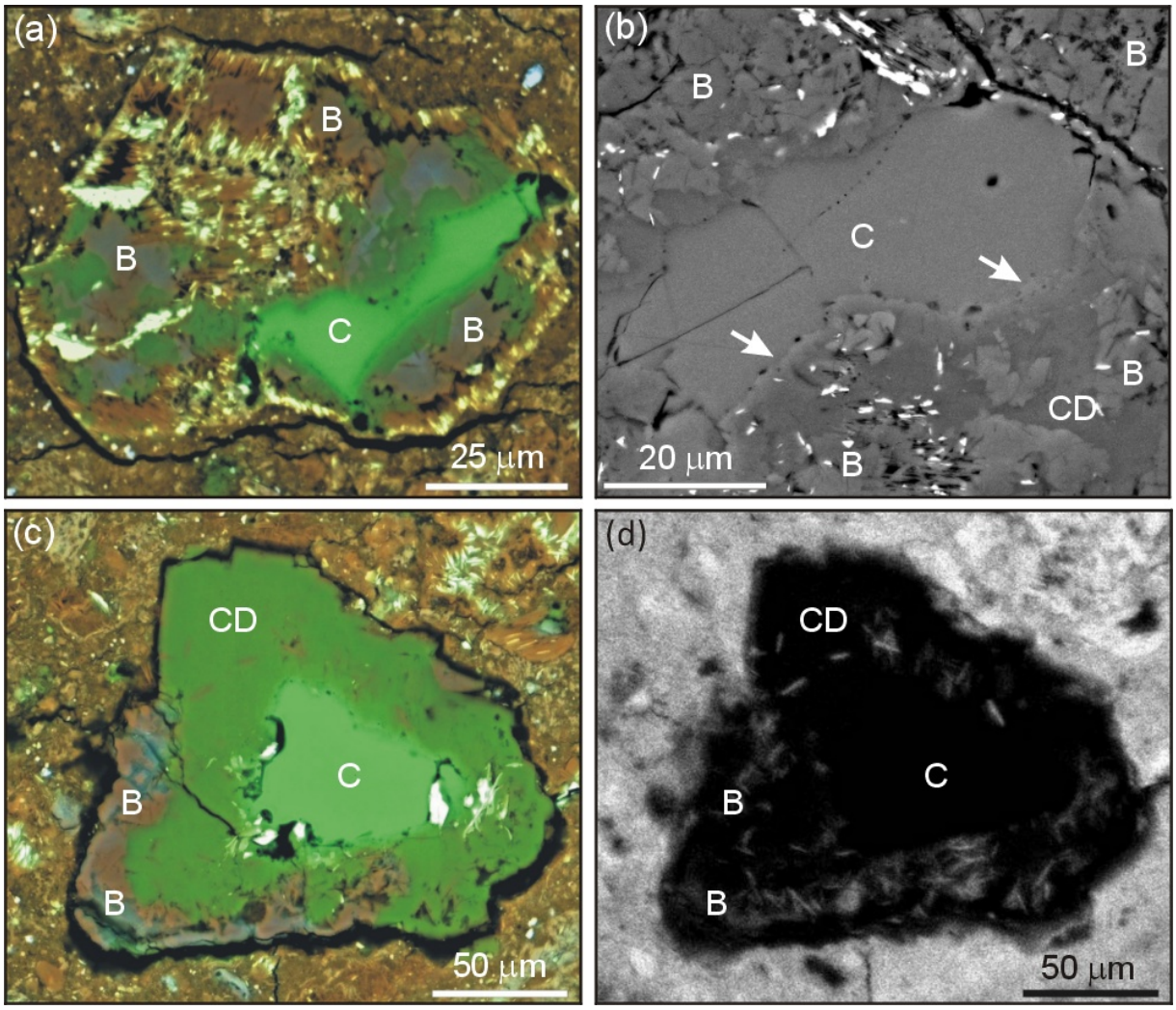

Figure 5. (a) Multielement X-ray map of an intact polymineralic grain. Breunnerite (B) occurs around its margins and is coloured brown with a blue tinge (the blue areas being richer in Fe), calcite (C, light green) is in the centre and a selvage of Ca-poor dolomite (dark green) lies between. The interface between Ca-poor dolomite and calcite is rounded and microporous. The grain contains considerable amounts of phyllosilicate (brown) intergrown with pentlandite (white). (b) BSE image of the centre of a polymineralic grain. The euhedral breunnerite crystals (B) contain phyllosilicate inclusions. Breunnerite is overgrown by Ca-poor dolomite (CD) whose interface with inclusion-free calcite (C) is delineated by a microporous Ca-rich zone (arrowed). White grains are Fe,Ni sulphides encrusting phyllosilicate crystals. (c) Multielement X-ray map of a polymineralic grain that has lost most of its rim so that breunnetite (B, light brown) remains only on the lower left hand side of the grain. Between breunnerite and calcite (C, light green) in the grain centre is Ca-poor dolomite (CD, dark green). Small white patches are Fe,Ni sulphides. (d) Si K_α X-ray map of the grain in (c). This map shows that the phyllosilicate fibres (white) are abundant as inclusions in the Ca-poor dolomite (CD) but are less common in breunnerite (B) and absent from the calcite (C).

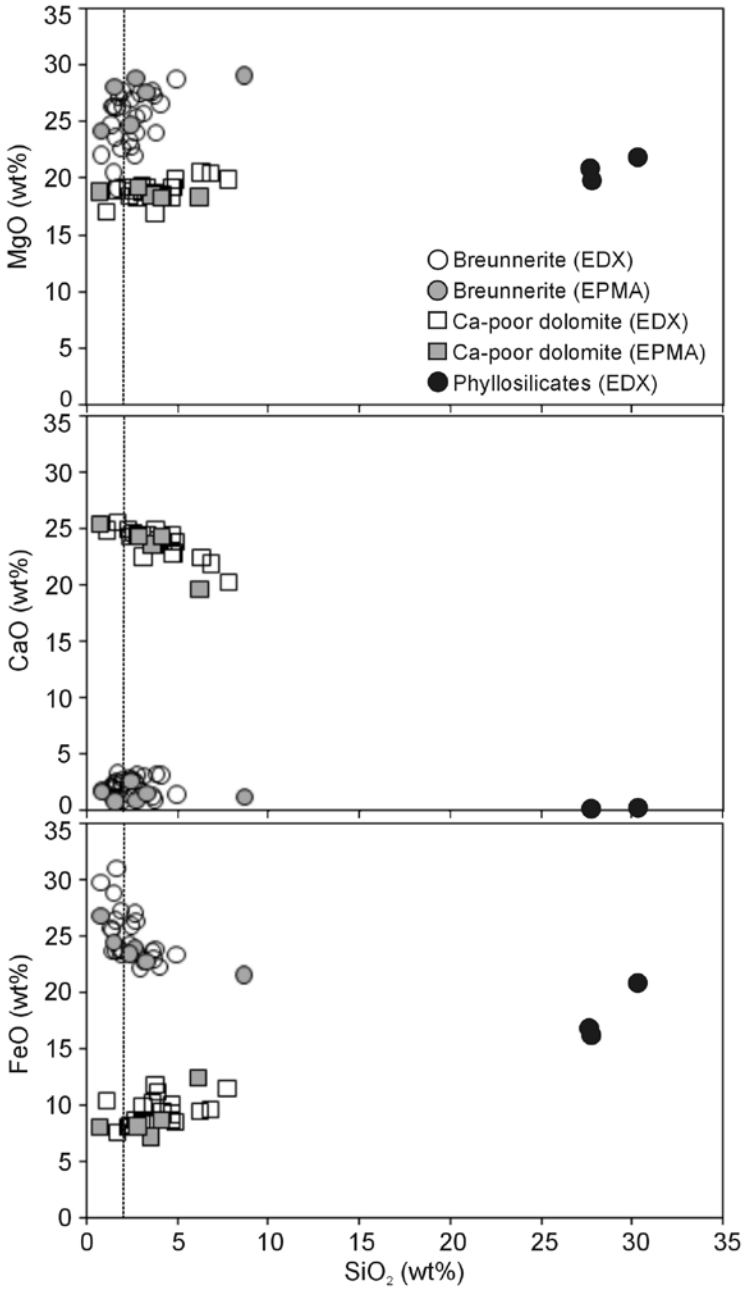

Figure 6. Plots showing the compositions of breunnerite, Ca-poor dolomite, and patches of coarsely crystalline Mg-Fe phyllosilicates that were free of intergrown sulphide or carbonate. The dashed lines indicate the 2 wt% SiO_2 threshold used in the calculations of mean carbonate mineral compositions. Data were obtained by both EDX and EPMA.

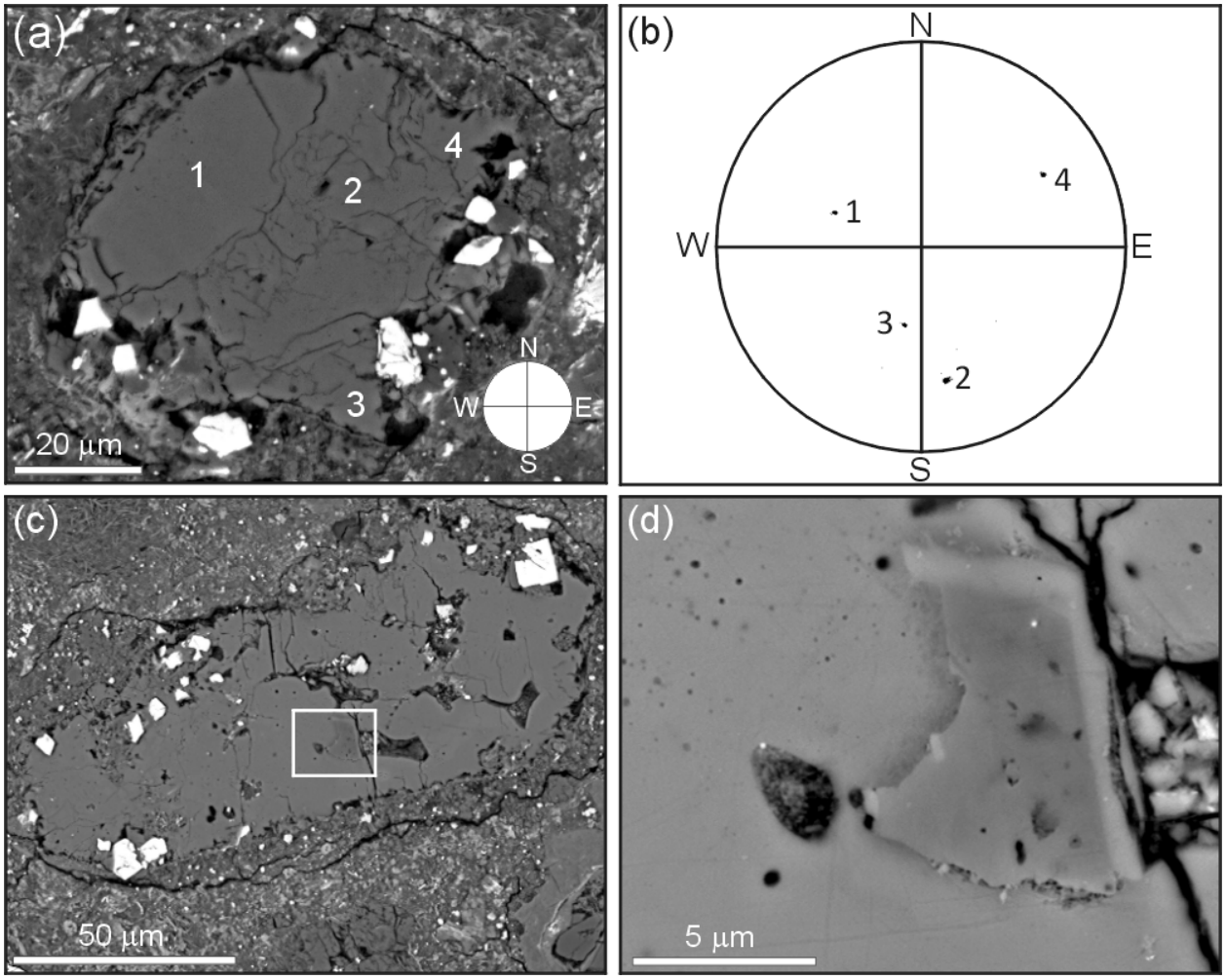

Figure 7. (a) BSE image of a polycrystalline calcite grain that is rimmed by equant sulphides (white). The inset shows reference directions used for EBSD. (b) Pole figure constructed from an EBSD map of the grain in (a). On the figure are plotted the orientations of the *c* axes of the subgrains numbered 1-4 in (a). The orientation of the pole figure relative to the image is shown by the inset in (a). (c) BSE image of a calcite-rich bimineralic grain with euhedral Fe,Ni sulphides (white) around its edge. (d) BSE image of a dolomite inclusion that occurs in the boxed area in (c). Note the ragged interface between the dolomite and calcite on the left hand edge of the inclusion but on its right hand edge the dolomite has a euhedral termination and is compositionally zoned.

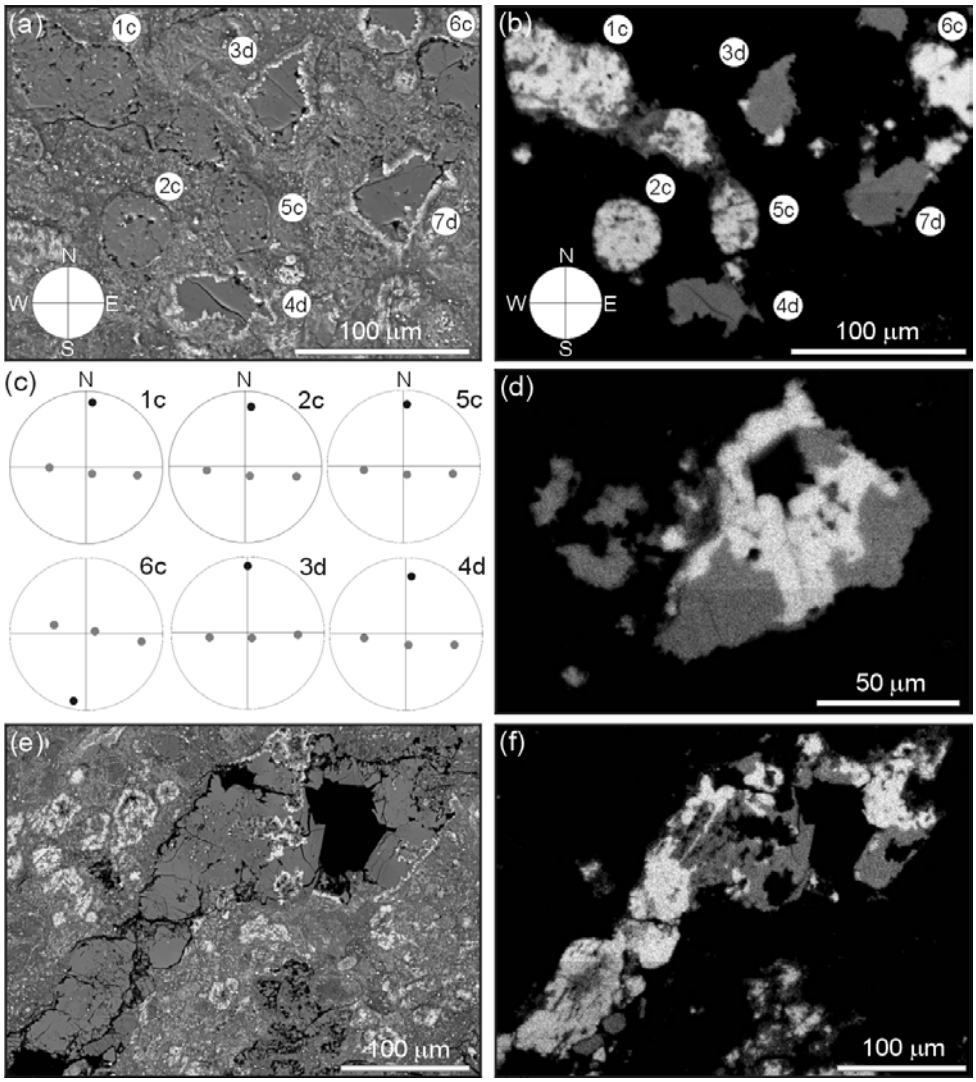

Figure 8. (a) BSE image of a carbonate cluster containing dolomite grains (3d, 4d, 7d) and calcite-rich bimineralic grains (1c, 2c, 5c and 6c). Of these grains 3d, 4d and 7d were analysed for the ^{53}Mn–^{53}Cr work. The inset shows EBSD reference directions. (b) Ca K_α X-ray map of (a) highlighting the distribution of calcite (white) and dolomite (mid grey). The matrix is black. The calcite-rich bimineralic grains in the middle and left of the image contain small inclusions of dolomite. (c) Pole figures showing the orientation of the *c* axis (black circle) and three *a* axes (grey circles) of six of the grains in the carbonate cluster, as determined by EBSD. These results show that all of grains have essentially the same crystallographic orientation with their *c* axis aligned close to the plane of the thin section and nearly north-south relative to the images in (a) and (b). (d) Ca K_α X-ray map of a bimineralic grain that contains approximately equal proportions of calcite (white) and dolomite (mid grey). The interface between the two minerals is mostly planar and parallel to dolomite cleavage planes. (e) BSE image and (f) Ca K_α X-ray map of a bimineralic calcite-dolomite vein. In (f) the calcite is white, the dolomite is mid grey and the matrix is black. Note in (e) that the phyllosilicate–sulphide rims occur only where vein dolomite, but not calcite, is in contact with the meteorite matrix.

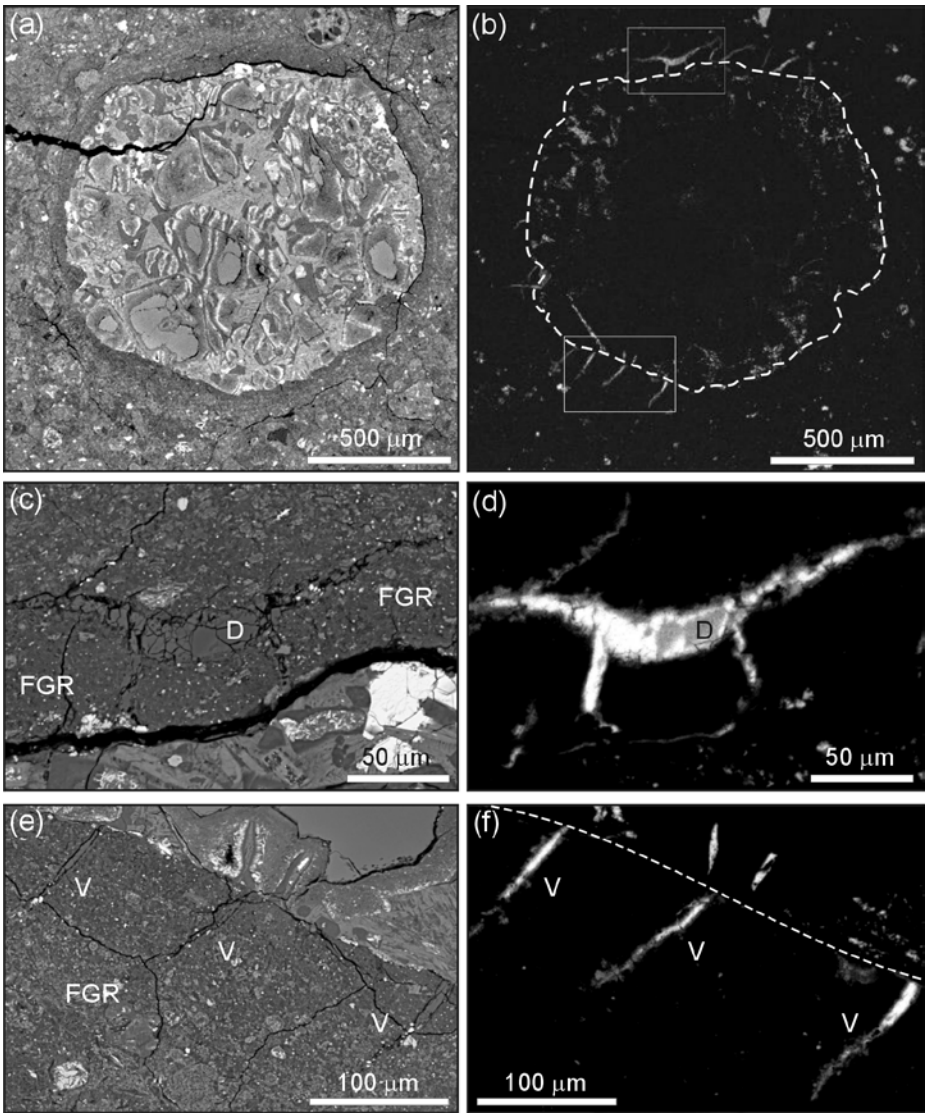

Figure 9. (a) BSE image of an aqueously altered chondrule whose narrow fine-grained rim contains carbonate veins. Most of the original constituents of the chondrule have been replaced by phyllosilicates, although some anhydrous crystals remain in its lower part. (b) Ca K_α X-ray map of (a) showing that Ca is concentrated in outer parts of the chondrule (whose edge is delineated by a dashed white line), and is also present within veins that cross-cut two sections of the fine-grained rim. Most of these veins are aligned approximately normal to the edge of the chondrule and are elongate NE-SW relative to the image. (c) BSE image of the upper boxed area in (b) showing porous and polycrystalline veins cross-cutting the fine-grained rim (FGR). Most crystals are calcite but dolomite (D) occurs in the centre of the largest vein. (d) Ca K_α X-ray map of (c) highlighting the calcite (white) and dolomite (D, grey). (e) BSE image of the lower boxed area in (b) showing three calcite veins (V) within the fine-grained rim (FGR) whose long axes are oriented normal to the outer edge of the chondrule. (f) Ca K_α X-ray map of (e) highlighting the locations of the three veins of calcite (white). The grey borders to the veins are areas with lower Ca X-ray counts owing to fine-scale intergrowth of the rim materials with calcite. The chondrule edge is delineated by the dashed white line.

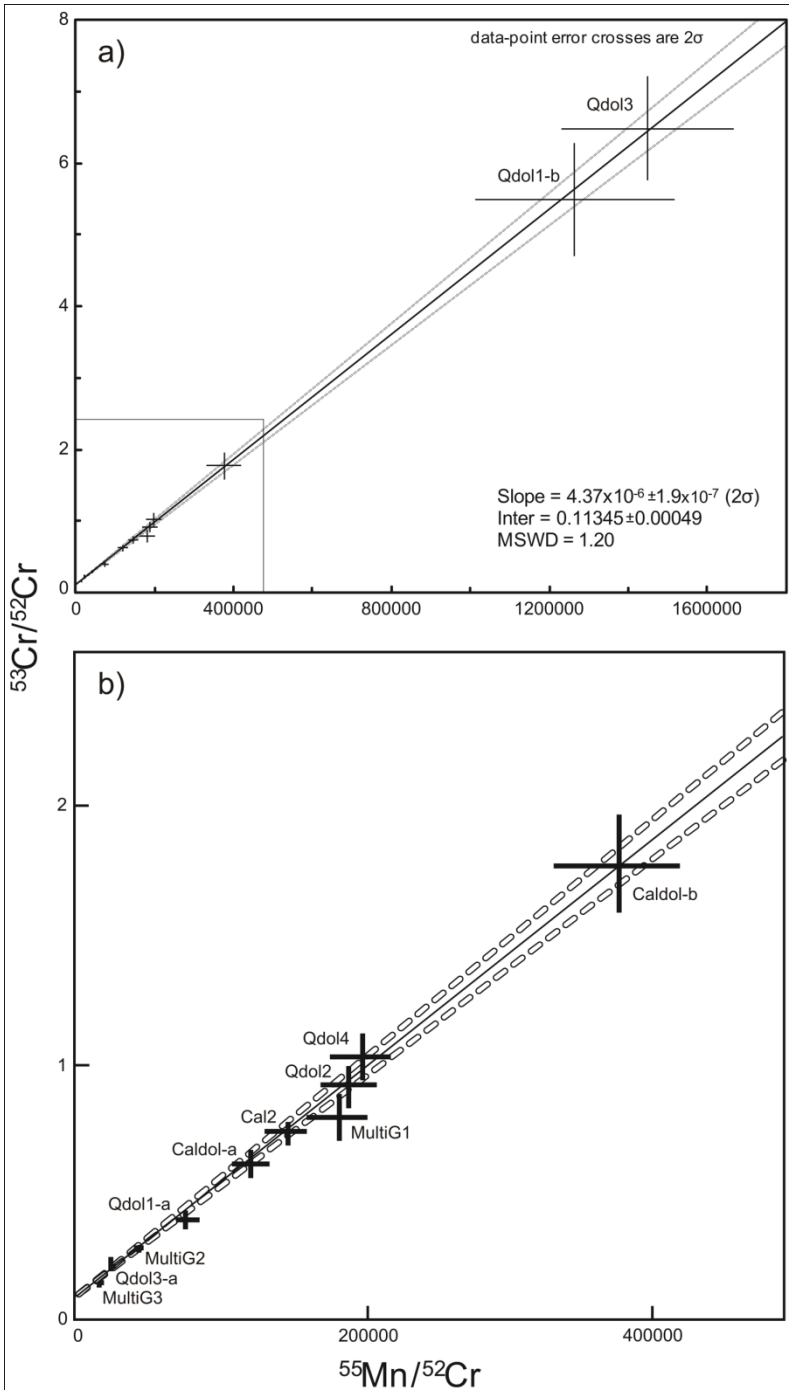

Figure 10. Mn–Cr evolution diagram for nine dolomite grains in QUE 93005. The values for each grain are listed in Table 1. An expanded-scale view of the lower left-hand corner of (a) is shown in (b). All grains fall within error of a single isochron, implying that they all formed over a short time interval with similar initial $^{53}Mn/^{55}Mn$ ratios of $4.37\times10^{-6}\pm1.9\times10^{-7}$ (2σ).

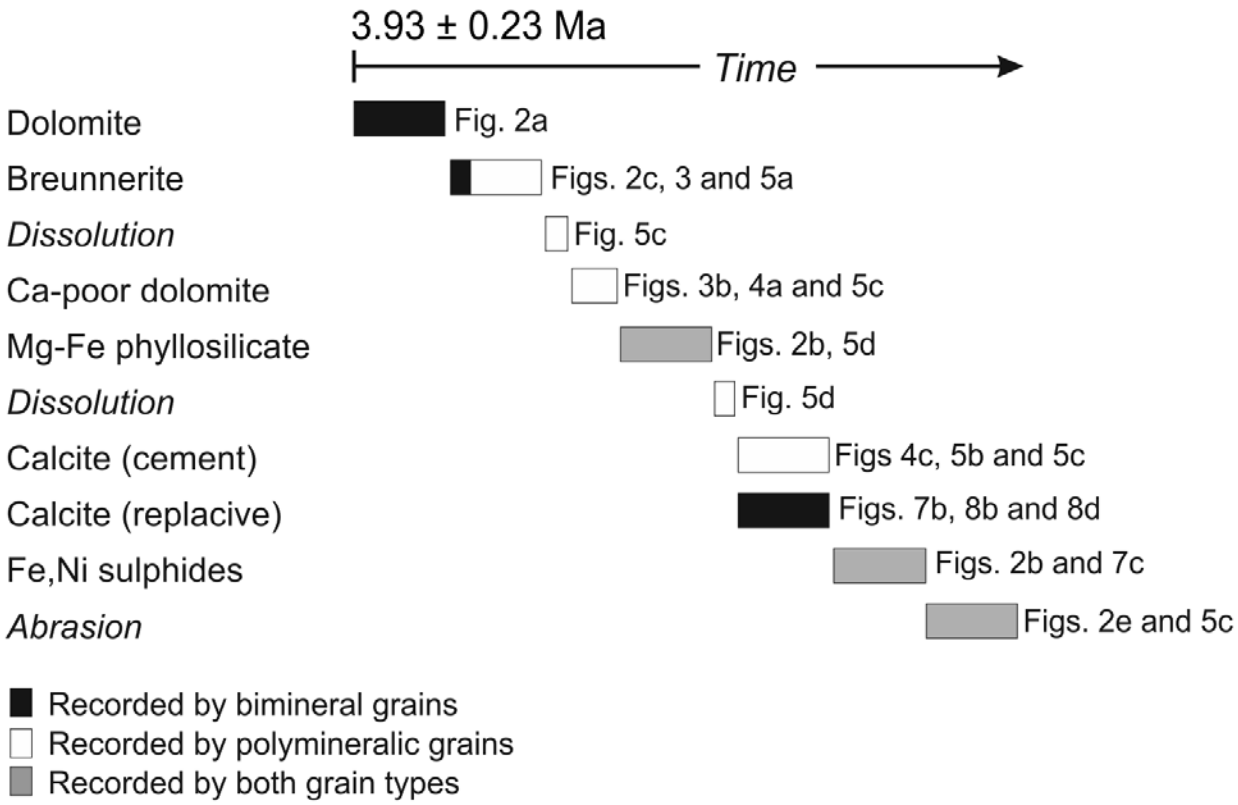

Figure 11. The chronology of mineralisation and related processes as recorded by the bimineralic and polymineralic grains. The figures that illustrate the timing of each event are also indicated.

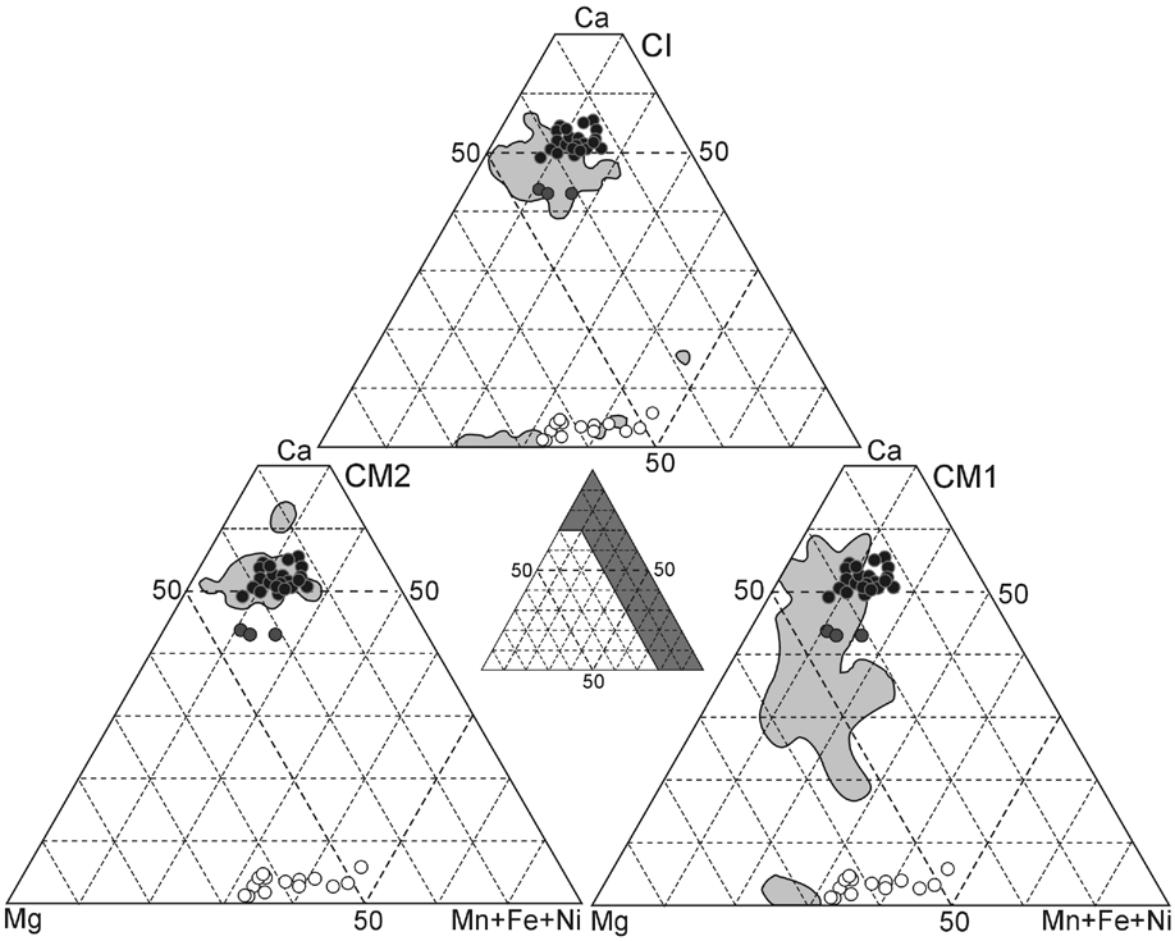

Figure 12. Ternary diagrams showing the compositions (mole%) of QUE 93005 dolomite (black circles), breunnerite (white circles) and Ca-poor dolomite (dark grey circles). Only plotted are those breunnerite and Ca-poor dolomite analyses with < 2 wt% SiO_2. The light grey areas indicate the compositional ranges of carbonates in other CM2s (lower left plot), the CM1 meteorites ALH 84034/84051 and EET 83334 (lower right) and in the CI meteorites (top). CM2 data from Johnson and Prinz (1993), Riciputi et al. (1994) and de Leuw et al. (2010); CM1 data from Zolensky et al. (1997) and Tyra et al. (2010a); CI data from Johnson and Prinz (1993), Riciputi et al. (1994) and Endress and Bischoff (1996).

Table 1
Isotopic compositions of nine dolomite grains in QUE 93005 and the average matrix analysis.

Grain identifier	Grain mineralogy	$(^{53}Cr/^{52}Cr) \pm 2\sigma$	$(^{55}Mn/^{52}Cr) \pm 2\sigma$
Qdol3[a]	Monomineralic	0.238 ± 0.022	21500 ± 1890
Qdol3[b]	Monomineralic	6.492 ± 0.730	1450000 ± 218000
Qdol1[a]	Monomineralic	0.407 ± 0.034	73400 ± 7420
Qdol1[b]	Monomineralic	5.494 ± 0.791	1260000 ± 253000
Qdol2	Monomineralic	0.924 ± 0.077	185000 ± 19500
MultiG3	Monomineralic*	0.164 ± 0.005	12600 ± 1120
MultiG1	Monomineralic*	0.805 ± 0.089	180000 ± 10500
MultiG2	Bimineralic*	0.295 ± 0.015	40500 ± 3610
Caldol[a]	Bimineralic	0.630 ± 0.052	118000 ± 11900
Caldol[b]	Bimineralic	1.779 ± 0.183	375000 ± 44200
Qdol4	Bimineralic	1.033 ± 0.087	195000 ± 20400
Cal2	Bimineralic	0.746 ± 0.046	143000 ± 13200
Average matrix[1]	n/a	0.113 ± 0.001	0.872 ± 0.246

[1]The average composition of 14 matrix analyses. The average $(^{53}Cr/^{52}Cr)$ ratio of the matrix was assumed to be the terrestrial ratio (see text). The errors are the standard errors in the means. *Grains occur in the cluster in Figure 8a. Superscipts [a] and [b] denote duplicate analyses.